THESIS FOR THE DEGREE OF DOCTOR OF PHILOSOPHY

Melt Spun Piezoelectric Textile Fibres - an Experimental Study

ANJA LUND

Department of Materials and Manufacturing Technology

CHALMERS UNIVERSITY OF TECHNOLOGY

Gothenburg, Sweden 2013

Melt Spun Piezoelectric Textile Fibres
- an Experimental Study
ANJA LUND
ISBN 978-91-7385-889-2

Doktorsavhandlingar vid Chalmers tekniska högskola
Ny serie nr 3570
ISSN 0346-718X

Department of Materials and Manufacturing Technology
Chalmers University of Technology
SE - 412 96 Göteborg
Sweden
Telephone: +46 (0)31 772 10 00

The Swedish School of Textiles
University of Borås
SE - 501 90 Borås
Sweden
Telephone: +46 (0)33 435 40 00

Cover: Piezoelectric fibres and the electrical signal generated by them
(photo: Roger Sagdahl)

Chalmers Reproservice
Gothenburg, Sweden 2013

Because it's there.

George Mallory

Piezoelektriska textilfibrer tillverkade genom smältspinning

ANJA LUND

Institutionen för Material- och tillverkningsteknik
Chalmers Tekniska Högskola

SAMMANFATTNING

Denna avhandling beskriver tillverkning och provning av piezoelektriska textilfibrer. Ett piezoelektriskt material har förmågan att generera en elektrisk spänning när det deformeras och denna egenskap kan återfinnas hos olika typer av material såsom keramer, mineraler och polymerer. Polyvinylidenfluorid (PVDF) uppvisar, enligt vad som är känt idag, den tydligaste piezoelektriska effekten bland polymererna. Dock måste PVDF bearbetas under vissa betingelser för att bli piezoelektrisk.

Undersökningen visar att det är möjligt att tillverka piezoelektriska bikomponentfibrer genom smältspinning, vilken är en vanligt förekommande och relativt enkel metod för fiberframställning. Fibrerna måste kallsträckas under spinningen – detta gör att en polär kristallstruktur bildas i polymeren. Fibrerna måste också förses med elektroder, vilket här åstadkommits genom att tillverka bikomponentfibrer med en kärna-hölje-struktur. Fiberns kärna utgörs av en blandning av en polymer och kol (kimrök) vilket gör den elektriskt ledande; därmed kan den utgöra en inre elektrod. Höljet består av PVDF som då utgör den piezoelektriska komponenten. En yttre elektrod kan påföras efter spinningen som en konduktiv beläggning.

De färdiga fibrerna reagerar på deformation såväl som temperaturförändringar, och förväntas vara användbara som sensorer i diverse tillämpningar. De små och flexibla piezoelektriska fibrerna bör kunna integreras som miniatyrsensorer i olika typer av strukturer eller plagg, utan att påverka dess form, utseende eller komfort.

Sökord: polyvinylidenfluorid, PVDF, fiber, smältspinning, röntgendiffraktion av polymerer, piezoelektricitet, smarta textilier

Melt Spun Piezoelectric Textile Fibres
- an Experimental Study

ANJA LUND

Department of Materials and Manufacturing Technology
Chalmers University of Technology

ABSTRACT

The manufacturing and characterisation of piezoelectric textile fibres are described in this thesis. A piezoelectric material is one that generates an electric voltage when deformed, a property which exists in a number of materials. The polymer with the strongest known piezoelectric effect today is poly(vinylidene fluoride) (PVDF), however it must be processed under certain conditions to become piezoelectric.

This study shows that piezoelectric bicomponent PVDF-based fibres can be produced by melt spinning, which is a common and relatively simple fibre spinning method. The melt spinning process must include cold drawing, as this introduces a polar crystalline structure in the polymer. The fibres must also be electroded, which is done by producing bicomponent fibres with a core-and-sheath structure. The core is electrically conductive and constitutes an inner electrode consisting of a carbon black/polymer compound, whereas the sheath is PVDF and constitutes the piezoelectric component.

Being sensitive to both deformation and temperature changes, these fibres are anticipated to be useful in a number of sensor applications. The flexibility and small size of the fibres makes it possible to include them as miniature-sensors in structures or garment without affecting the shape or comfort.

Keywords: poly(vinylidene fluoride), PVDF, fibre, melt spinning, crystal structure, X-ray diffraction of polymers, piezoelectric polymer, smart textile

LIST OF PUBLICATIONS

This thesis is based on the work contained in the following papers, referred to by Roman numerals in the text:

I *Melt spinning of poly(vinylidene fluoride) fibers and the influence of spinning parameters on β-phase crystallinity*
A. Lund and B. Hagström
Journal of Applied Polymer Science, Vol. 116, 2685-2693 (2010)

II *Enhancement of β phase crystals formation with the use of nanofillers in PVDF films and fibres*
A. Lund, C. Gustafsson, H. Bertilsson, R. W. Rychwalski
Composites Science and Technology, Vol. 71, 222-229 (2011)

III *Melt spinning of β-phase poly(vinylidene fluoride) yarns with and without a conductive core*
A. Lund and B. Hagström
Journal of Applied Polymer Science, Vol. 120, 1080-1089 (2011)

IV *Piezoelectric polymeric bicomponent fibers produced by melt spinning*
A. Lund, C. Jonasson, C. Johansson, D. Haagensen, B. Hagström
Journal of Applied Polymer Science, Vol. 126, 490-500 (2012)

V *Poling and characterization of piezoelectric polymer fibers for use in textile sensors*
E. Nilsson, A. Lund, C. Jonasson, C. Johansson, B. Hagström
Accepted for publication in
Sensors & Actuators: A. Physical

Contributions to the appended papers

The author's contributions to the appended papers are as follows:

Paper I: Planned and conducted the experiments, wrote main part of the paper.

Paper II: Planned and conducted the experiments together with C. Gustafsson. Took part in writing of the paper.

Paper III: Planned and conducted the experiments together with B. Hagström. Wrote main part of the paper.

Paper IV: Planned the experiments together with the co-authors. Conducted DSC, XRD and viscosity measurements. Responsible author of the paper.

Paper V: Took part in planning, analysis and writing of the paper.

Additional publications, not included in the thesis:

MWNT reinforced melamine-formaldehyde containing alpha-cellulose
L. Licea-Jiménez, P. –Y. Henrio, A. Lund, T. M. Laurie, S. A. Pérez-García, L. Nyborg, H. Hassander, H. Bertilsson, R. W. Rychwalski
Composites Science and Technology, 67, 844-854 (2007)

Appeared on *Kunskapskanalen (SVT*) in a documentary on carbon nanotube research, May 2007

Nanotechnology for textile applications
A. Lund and H. Bertilsson
The Nordic Textile Journal, Smart Textiles Special Edition, 116-125, (2008)

Analysis of the torsion angle distribution of poly(vinylidene fluoride) in the melt
K. C. Satyanarayana, M. Bohlén, A. Lund, R. W. Rychwalski, K. Bolton
Polymer, Vol. 53, 1109-1114 (2012)

Polymer based multi-component piezoelectric fibers and yarns
B. Hagström, A. Lund, E. Nilsson
Patent application No. 1330031-4. Filed April 2013.

TABLE OF CONTENTS

1. Introduction

1.1 Background

A piezoelectric material is one that generates an electric voltage when deformed and, vice versa, deforms when an electric voltage is applied to it. Such materials are used in a number of everyday applications such as microphones, speakers, beepers, accelerometers and pressure sensors. The piezoelectric effect exists in ceramics, minerals and polymers, and is due to a non-symmetric atomic arrangement that results in a polar crystal structure.

The polymer known to have the highest piezoelectric effect is poly(vinylidene fluoride) (PVDF), and sensors based on PVDF are commercially available in the form of films or coaxial cables. In the last decade, several studies are presented where PVDF films are added to a textile structure for measuring for example heart beat or body motion. In such applications, it should be advantageous to instead use PVDF in fibre form; a fibre can be easily knitted or woven thus being fully integrated into the textile. Being very thin and flexible, a fibre could further be embedded in or applied on the surface of various types of constructions without affecting their shape or mechanical properties.

PVDF is thermoplastic, has good mechanical properties and has a high resistance to chemicals. Besides its piezoelectric applications, PVDF is used for example in pipes and electrical insulation. It can be melt spun and used as sutures and fishing lines, however for use as a piezoelectric material PVDF must be processed so that it forms a polar crystal structure, known as the β phase. The melt spinning parameters can be expected to affect the crystal formation, but presently only a few studies on this topic are available.

Further the β phase must be oriented so that the material is polarised on a macroscopic level; this is done in a process known as poling which involves applying a very high electric field to the polymer. Both the poling and the harvesting of the piezoelectric effect require electrodes, or electrically conductive surfaces, to be added to the fibre. Whereas the commercially available PVDF-films are electroded simply by metallisation of its surfaces, the electroding of fibres must be regarded as a new challenge.

1.2 Aim

The aim of the present study is to produce and characterise piezoelectric fibres suitable for integration into textile materials. The main research questions addressed here are:

1. How should PVDF be processed in order to produce fibres with a large degree of β phase crystallinity?
    a. Which melt spinning parameters are suitable?
    b. Does the incorporation of carbon nanotubes have a positive effect on β phase formation?
2. How should the PVDF-fibres be polarised?
    a. How are electrodes conveniently added to the fibre?
    b. Can poling be carried out as a continuous process?

1.2.1 Delimitations

The piezoelectric polymer used is PVDF from one supplier and the processing method is melt spinning.

2. Piezoelectricity

Piezoelectricity literally means pressure electricity; a piezoelectric material generates an electric field when deformed and, vice versa, deforms when an electric field is applied to it. These mechanisms are known as the direct and the reverse piezoelectric effect. Piezoelectricity is characteristic of materials with a non-symmetric atomic structure – such materials exist among ceramics, minerals and polymers [1]. These materials may also be pyroelectric, meaning that they generate an electric field in response to a temperature change. One early use of piezoelectric ceramics was in sonar in the early 1920s, wherein the reverse and direct piezoelectric effect were both used to emit and receive ultrasonic signals detecting underwater objects such as submarines [2].

2.1 Piezoelectric polymers

The piezoelectric effect in polymers was first noticed in natural material such as wood, starch and horn. A demonstration of the piezoelectric effect in tendon, bone and whalebone was conducted by Fukada in 1959 where these materials were used as the active component in gramophone pickups [1]. The piezoelectric effect in polarised poly(vinylidene fluoride) (PVDF), polyethylene (PE), poly(tetra fluoroethylene) (PTFE) and polycarbonate (PC) was first reported by Kawai in 1969 [3]. The effect was significantly higher and more stable over time in PVDF than in the other polymers. Since then, a relatively strong piezoelectric effect has been reported in polyamide (PA) [4] and poly-L-lactic acid (PLLA) [5], but PVDF and its copolymers still have the highest known piezoelectric coefficients among polymers; the typical piezo strain constant (see section 4.3.4) for a PVDF film is d_{31}=23 pC/N compared to for example d_{31}=2.2 pC/N for a PA11 film [4].

In the 1970s hydrophones, microphones, headphones and tweeters based on PVDF films were commercialised [1]. PVDF can now also be purchased in the form of thin films or coaxial cables for sensor and actuator applications and recently, smart textiles were designed based on such films. A few examples include sensors for cardio-respiratory monitoring during sleep to be placed under the bed sheets [7, 8] or integrated into a belt [9], and energy-harvesting devices inside a shoe [10].

2.2 PVDF basics

Apart from being piezoelectric, PVDF has attractive properties such as a high resistance to chemicals and UV-light, biocompatibility and good mechanical properties. It is commonly used in pipes and as the insulating layer in electrical cables, and exists in fibre form for sutures and fishing lines. Table 1 lists general properties (as given by the supplier [11]) for the three grades of PVDF used in this study. Its repeating unit is shown in Figure 1.

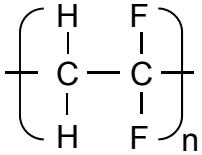

Figure 1 *The repeating unit of PVDF*

Table 1 *General properties of PVDF*

	Solef 1010	Solef 1008	Solef 1006
Molecular weight M_n/M_w (Da)	153/352	114/244	
MFI (g/10 min)*	2	8	40
Density (g/cm^3)	1.78		
Melting point (°C)	171-172		
Elastic modulus (GPa)	1.3-2.2		
Stress at break (MPa)	40		
Volume resistivity (Ωcm) at 23°C		$> 10^{14}$	
Breakdown voltage (kV)**		< 2.5	
Dielectric strength (kV/mm)**		100	
Dielectric constant (ε_r)***	9		

*MFI: Melt flow index at 230°C under a load of 2.16 kg

**Valid for uniaxially drawn Solef 1008 films, 25 µm thick

***Dielectric constant at 23°C and 60 Hz

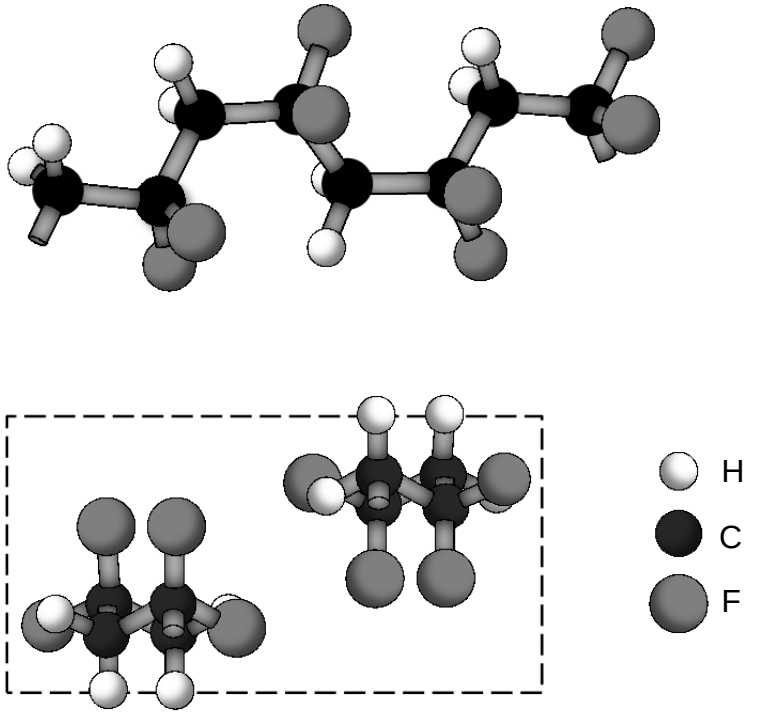

Figure 2 *The α phase chain conformation and crystal unit cell of the PVDF molecule*

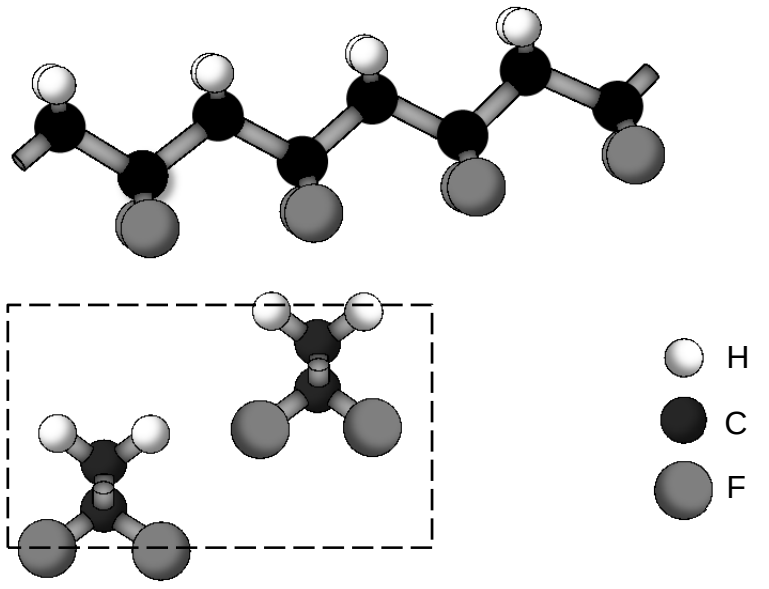

Figure 3 *The β phase chain conformation and crystal unit cell of the PVDF molecule*

PVDF is semi-crystalline and polymorphic; it crystallises in at least four different forms or phases denoted α, β, γ and δ and the piezoelectric effect is due to a high net polarity in the β phase crystallites. The crystal phase formation is well explored in the case of PVDF films [12-15] and there is an agreement that whereas α phase is formed during crystallisation from the melt or in solution-cast films, β phase can be formed by mechanical deformation of α phase material. α phase polymer chains have a TGTG' (T = trans, G = gauche) conformation (Fig. 2) and β chains have an all-trans conformation (Fig. 3). The difference in electronegativity between the hydrogen and fluorine atoms introduces a high net polarity in the β phase unit cell perpendicular to the chain axis, so that the β phase unit cell can be regarded as a dipole. The α phase unit cell on the other hand is completely non-polar [16, 17]. Thus for piezoelectric applications, PVDF must be processed in such a way that β phase formation is promoted.

The γ and δ phases are less common; γ phase has a TTTGTTTG' conformation and is formed in PVDF crystallised at a high temperature and/or under a high pressure. The γ phase readily transforms into β when stretched [18]. The δ phase is a polar version of α and can be formed when α phase PVDF is subjected to a high electric field [18, 19]. The different chain conformations result in unit cells with different dimensions, given in Table 2. As the melt spinning process largely influences the structure of a fibre, the processing (spinning) parameters can be expected to influence the degree of crystallinity as well as the morphology. This is further discussed in section 3.4. In a different approach, the addition of nanoparticles may enhance β phase content, see section 3.5.

Table 2 *Unit cell dimensions for the different crystalline phases of PVDF*

		Unit cell dimensions (Å) [20]		
		a	*b*	*c*
Crystalline phase	α	4.96	9.64	4.62
	β	8.58	4.91	2.56
	γ	4.97	9.66	9.18
	δ	4.96	9.64	4.62

3. Melt spinning

3.1 A brief historical review

Melt spinning is the commercially most important fibre spinning process. The method is simple: solid polymer pellets are melted and pumped through a spinneret (die) with one or several holes. The extruded filament is then cooled and stretched in several steps before being collected on a bobbin (Fig. 4).

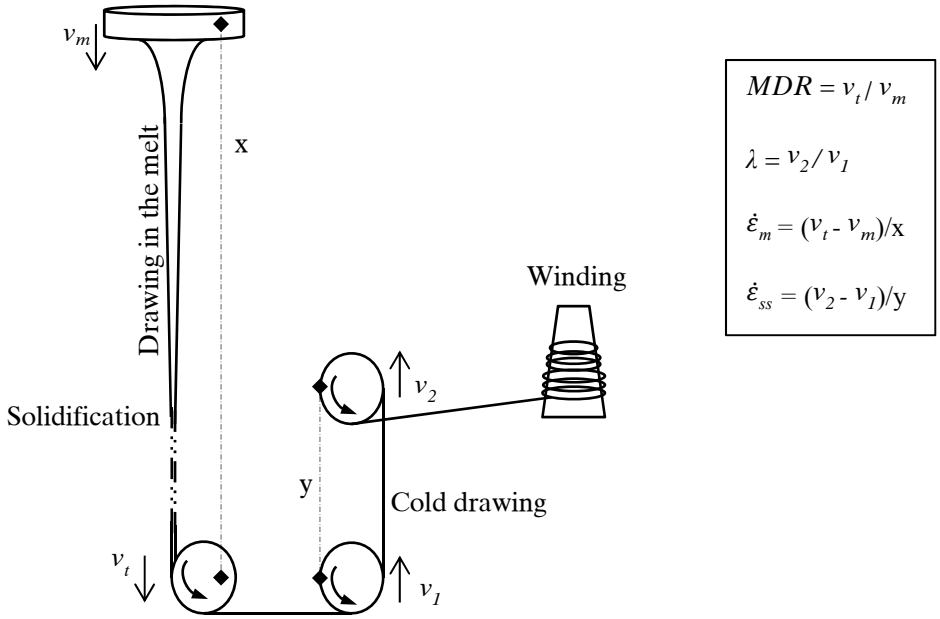

Figure 4 *The principle of melt spinning with the definitions of melt draw ratio (MDR), solid state draw ratio (λ), nominal melt draw rate ($\dot{\varepsilon}_m$) and solid state draw rate ($\dot{\varepsilon}_{ss}$).*

When the process was first introduced the great challenge was to develop polymers suitable for fibre formation through melt spinning. The pioneering work in this field is largely attributed to W. Carothers of the DuPont Company, who supervised the successful synthesis and melt spinning of polyamide 6.6 (known as Nylon) in 1935. In a further development of Carother's research, J. Whinfield and J. Dickson synthesised poly(ethylene therephtalate) (PET), or polyester, suitable for fibre spinning in 1941. The polyester fibres were eventually commercialised under the trademarks Terylene and Dacron [12-14]. The new, fully synthetic fibres were received with enthusiasm as they demonstrated new qualities compared to the natural fibres, such as high

mechanical strength and low moisture absorption. This allowed them to retain their dimensions and mechanical strength when wet, which resulted in an increased wear life and “ease of care” [13, 15].

Prior to these discoveries, some hundreds of polymers had been made and rejected due to problems such as low melting point and thermal instability. A few principles of fibre-forming polymers were founded: (i) the polymer should consist of very large molecules, (ii) the polymer should be capable of crystallising; therefore linear and symmetric chains are preferred and (iii) three-dimensional polymers are unsuitable. By the 1950s melt spinning was a firmly established method for production and it was suggested that from now on the research towards new products would be carried out by fibre and textile manufacturers, rather than by the chemical industry [13]. This was not entirely correct; for example the introduction of highly spinnable polyolefins was yet to come [16].

An example of development in the fibre spinning technology was the introduction of spinnerets with non-circular orifices in the 1940s, producing fibres with a wide range of cross-sections such as hollow, star-shaped or triangular, thus manipulating their mechanical properties and appearance [17].

A closely related development is that of biconstituent or bicomponent fibres. The initial purpose of bicomponent fibres was to introduce the crimp already present in natural fibres; crimp facilitates yarn spinning and affects the aesthetics and comfort of the final yarn. A self-crimping effect can be introduced to synthetic fibres by spinning them from two components with different shrinkage characteristics in a side-by-side arrangement, as was first demonstrated by spinning a fibre combining two different viscose solutions. The solutions were fed through the same spinneret hole, separated by a thin metallic plate [18]. A general method for spinning bicomponent multifilament in several configurations was later introduced. This method employed different configurations of plate mixers, feeding the spinning solution or melt through a series of laminated plates [19].

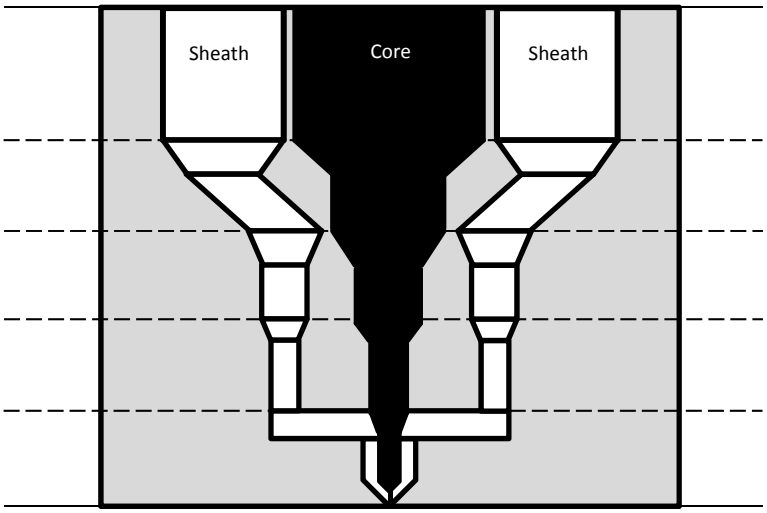

Figure 5 *Polymer melt distribution in one channel of the spinneret during bicomponent spinning*

Bicomponent fibres with a sheath/core configuration are suitable for combining attractive properties of two different components. For example, a rayon+nylon composite fibre can be imparted with the good mechanical properties of the nylon core and the high moisture absorption of the rayon sheath [20]. Generally speaking a very thin sheath of a different polymer could be useful in improving dyeability, changing the "hand" or affecting electrostatic properties. Bicomponent fibres can also be a good raw material for nonwovens where the sheath serves as the binder for thermal bonding [21].

In Papers III-V, the bicomponent sheath/core structure was used to produce fibres from compounds which are normally not spinnable due to highly elastic behaviour, as is further discussed in sections 3.2 and 3.3. The component with low spinnability was placed in the core, and the sheath consisted of PVDF. In our spinning line, the fibres were extruded through a spinneret, or spin pack, consisting of 5 layers of metal discs (Fig. 5).

3.2 Spinnability

A spinnable polymer melt is one that can be continuously extruded and drawn without breaking [17], thus it must be able to withstand considerable stress and extension. Three major modes of failure in a spin-line are identified (see Fig. 6): capillarity, ductile failure and fracture.

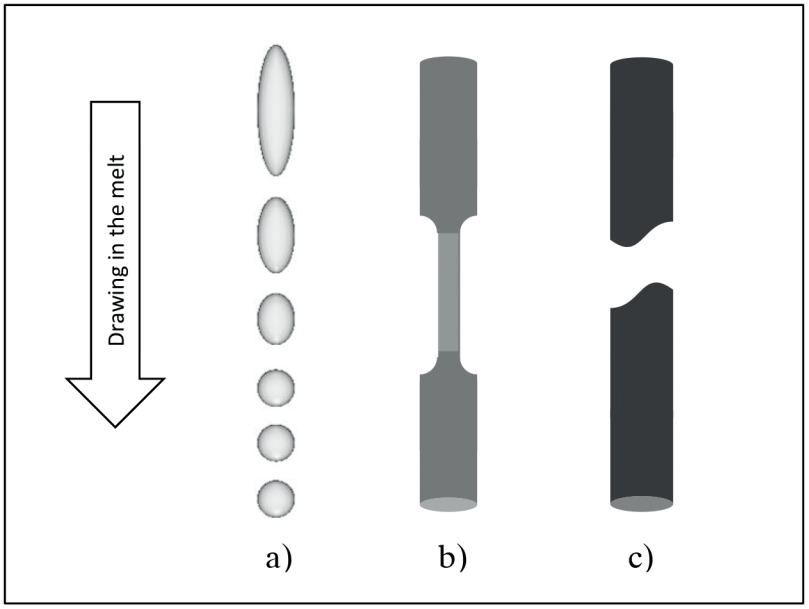

Figure 6 *Schematic illustrations of three mechanisms for spin-line failure:*
a) capillary break-up
b) ductile failure
c) fracture or cohesive failure

Capillarity refers to breakup of filaments into drops and is induced by surface tension, *i.e.* when forming new surfaces becomes more energetically favourable than maintaining the fibre form. Ductile failure occurs when a neck is introduced in the filament and grows to the point where the cross-section is reduced to zero. Fracture, or cohesive failure, means that the filament simply breaks [22]. In melt spinning, the polymer melts normally have a high enough molecular weight (MW) and viscosity to prevent capillary break-up. Instead, the filament may fracture if the spin-line stress is too high.

The necking mechanism in the melt can also cause spin-line instability at low draw ratios, especially if the melt is highly elastic. In this case a local "neck" may form, followed by an accumulation of material and a local large diameter portion in the filament. Proceeding down the spin-line,

the local accumulation adds extra force to the spin-line and induces another neck. This instability is known as draw resonance [23].

The spin-line stress is obviously related to the melt viscosity and draw-down velocity, but also to the extrusion conditions. In a viscoelastic polymer melt, the entire deformation history affects the developed spin-line stress. As the melt is pushed through a die the imposed strains will result in expansion of the melt (die swell) upon exit. The die design has a strong influence on the die swell and drawability. If the channel and/or the residence time is long enough the polymer melt will relax, and orientations from the contraction flow at the die entrance will decay prior to exiting so that swelling is reduced. A shorter residence time on the other hand can lead to significant die swell and reduction of the maximum melt draw ratio and speed [24]. A related distortion, sharkskin, is caused by cohesive failure near the surface. It is initiated at the die exit by the sudden axial acceleration of the melt layer near the capillary wall. For a given polymer, sharkskin will occur above a certain flow rate, the level of which is lower in a polymer with higher MW [25].

3.3 Melt spinning of PVDF

Our first melt spinning experiments were carried out with a relatively high MW grade PVDF (Solef 1010). Spinning was performed in a small scale using a capillary rheometer and compared to industrial melt spinning, MDR was high but the extrusion and drawing velocities were very low [Paper I]. First trials with the high MW grade PVDF in the large-scale pilot spinning equipment (Fig. 7) caused spin-line instabilities such as shark-skin and ductile fracture. These problems were overcome by using a lower MW-grade (Solef 1008) which was spinnable as mono-component fibres. However, introducing a core compound of polypropylene (PP) with 8.5 wt% carbon black (CB) again caused instabilities and spin-line break; the first bicomponent fibres could only be spun at low MDRs and with cold drawing at very low draw rates [Paper III]. Again, the PVDF was replaced with a grade (Solef 1006) with lower MW, and stable bicomponent fibre spinning could be realised [Paper IV]. The core polymer PP was replaced in order to enhance the conductivity, as further discussed in section 4.2. Two PE-type polymers were evaluated for this purpose: a copolymer PE (coPE) and a high density PE (HDPE). The melt spinning conditions used for the different equipment and grades are listed in Tables 3 and 4.

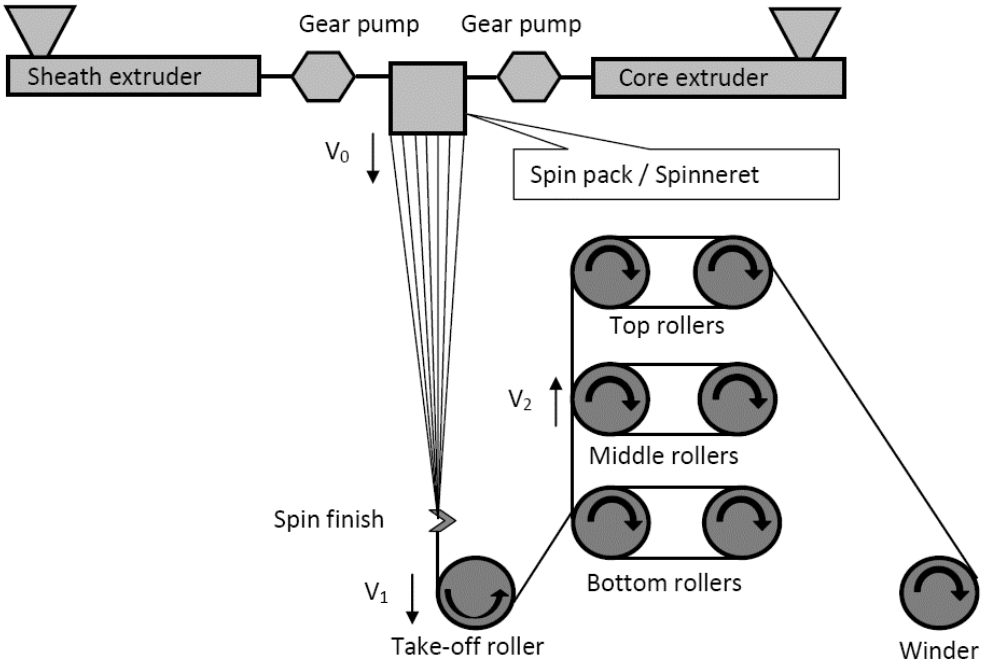

Figure 7 *Schematic of the bicomponent fibre spinning machine [from PaperIV]*

The maximum melt draw ratio and rate were lower in the large-scale pilot equipment (see Table 3) and this was due to the differences in extrusion rates and die geometries between the spinning machines. The pilot machine die consisted of a spin-pack with several layers, where the final capillary had a length-to-diameter (L/D) ratio of 2 compared to L/D = 40 in the rheometer. Thus the degree of pre-orientation in the melt was significantly higher in large-scale spinning.

Table 3 *Spinning parameters (drawing in the melt) in our experiments*

MFI_{PVDF}	v_m (m/min)	v_t (m/min)	MDR	$\dot{\varepsilon}_m$ (min^{-1})	Equipment	Paper
40	0.451	19 – 188	42 – 419	74 – 750	Rheometer	I
8	3.5 – 7.1	142 – 500	20 – 141	90 – 331	Pilot	III
8*	2.12 – 2.65	50	20 – 25	32	Pilot	III
2**	2.64	73 – 342	30 – 137	18 – 226	Pilot	IV
2***	5.27	98 – 116	20 – 23	62 – 74	Pilot	IV

* Bicomponent spinning with a CB/PP core

** Bicomponent spinning with a CB/coPE core

*** Bicomponent spinning with a CB/HDPE core

Table 4 *Spinning parameters (cold drawing) in our experiments*

MFI_{PVDF}	MDR	v_1 (m/min)	v_2 (m/min)	λ_{max}	$\dot{\varepsilon}_{ss}$ (min^{-1})	Cold-drawing method	Paper
40	42 – 419	3 – 6	6 – 18	6	7.6 – 38	Off-line	I
8	20 – 141	142 – 500	142 – 800	4	0 – 1356	In-line	III
8*	20 – 25	3	6 – 9	3	0 – 30	Off-line	III
2**	30 – 137	73 – 342	361 – 370	4.5	86 – 886	In-line	IV
2***	20 – 23	98 – 116	489	4.75	1147 – 1203	In-line	IV

* See Table 3 for definitions

3.4 Structure development in melt spinning

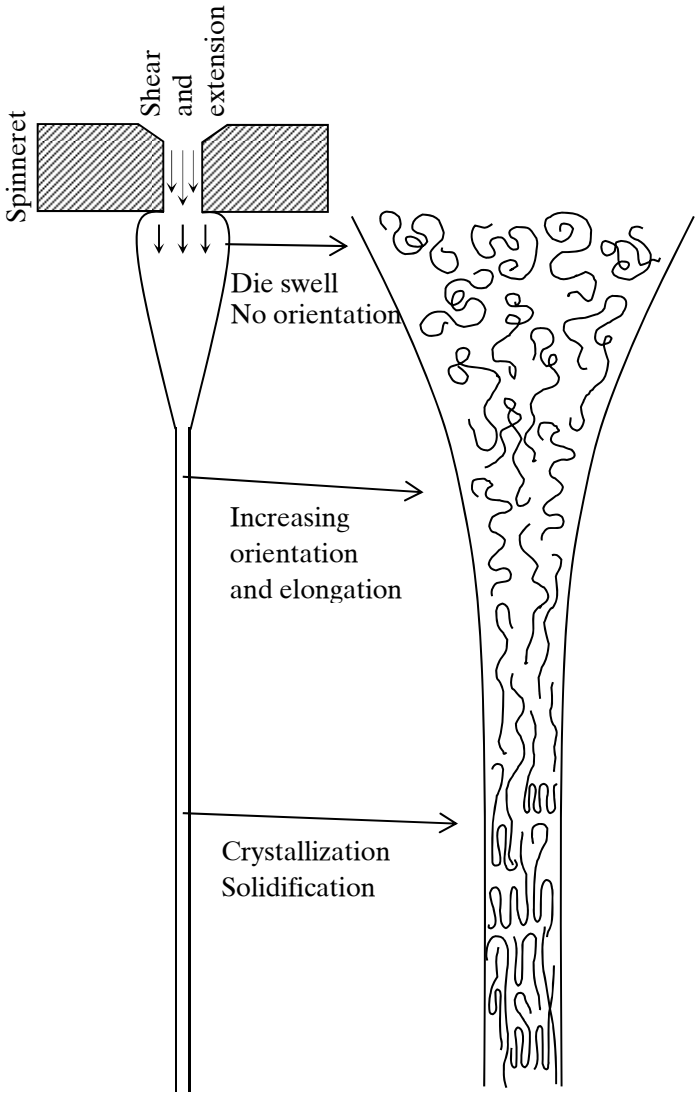

Figure 8 *Illustration of structure development during melt spinning (drawing in the melt), cf [21, 25]*

The process-structure-property relationship in polymer fibre processing was recognised early on; spinning parameters such as temperature and velocity strongly influence the final properties of melt-spun fibres. The molecular orientation introduced by drawing generally leads to an increase in both crystallisation temperature and crystallisation rate for a certain polymer [17, 26-29]. The determining factors for the degree of orientation are identified as spin-line stress, which stretches the melt, and

heat transfer, which cools the melt [27-29]. Their effect on the final degree of crystallinity can vary since both the degree of orientation and the cooling rate increase with take-up velocity. Thus at small orientations crystallinity decreases with increasing cooling rate (as in the case of un-oriented crystallisation) but at higher orientations the increase in crystallisation rate may compensate for the reduced crystallisation time, and higher or much higher degrees of crystallinity are found [17]. This mechanism makes it possible to spin crystalline PET-fibres with high speed spinning, even though PET is typically very slow to crystallise [30].

Crystallisation under orientation (Fig. 8) also affects the morphology; the spherulitic structure, common in polymers crystallised under quiescent conditions, are found in fibres only when spun at very low take up velocities. In melt-spun fibres, the shish-kebab crystalline structure is more common [21, 29]. The shish consists of extended polymer chains, oriented in the direction of flow, and the kebab is a lamellar structure oriented perpendicular to the orientation axis nucleated on and epitaxially grown from the shish [17]. Under weak orientations, the extended chains, or shishes, are very far apart. As the spin-line stress is increased, so is the rate of nucleation of shishes (more amorphous polymer is converted to shish) and the spacing between the shishes decreases [31].

After extrusion and drawing of the melt, there will typically be one or more processing steps in the spinning line where the fibres are cold-drawn. Cold drawing refers to drawing in the solid state, at a temperature T: $T_g < T < T_m$, where T_g is the glass transition temperature, and T_m is the crystal melting temperature. Prior to cold drawing the fibres exhibit poor mechanical properties, such as low stiffness, high strain to break and high irreversible extensibility. Cold drawing introduces an irreversible elongation on the macro-scale and, on the micro-scale, an extension and orientation of polymer chains and crystallites along the fibre axis, and the orientation increases with increasing draw ratio. The effect of cold drawing on the degree of crystallinity is difficult to predict; depending on the system the draw ratio and the draw rate are known to have both positive and negative correlations with the final degree of crystallinity [17].

3.4.1 Characterisation of the crystal structure in PVDF

The structure development in PVDF films is rather well described (see section 2.2), and the most common method for analysis is wide angle X-ray diffraction (WAXD) (from here on referred to as X-ray diffraction (XRD)) where a few maximum intensity peaks are used to identify the crystalline phase(s) present. One difficulty is that these peaks are partly overlapping (Fig. 9).

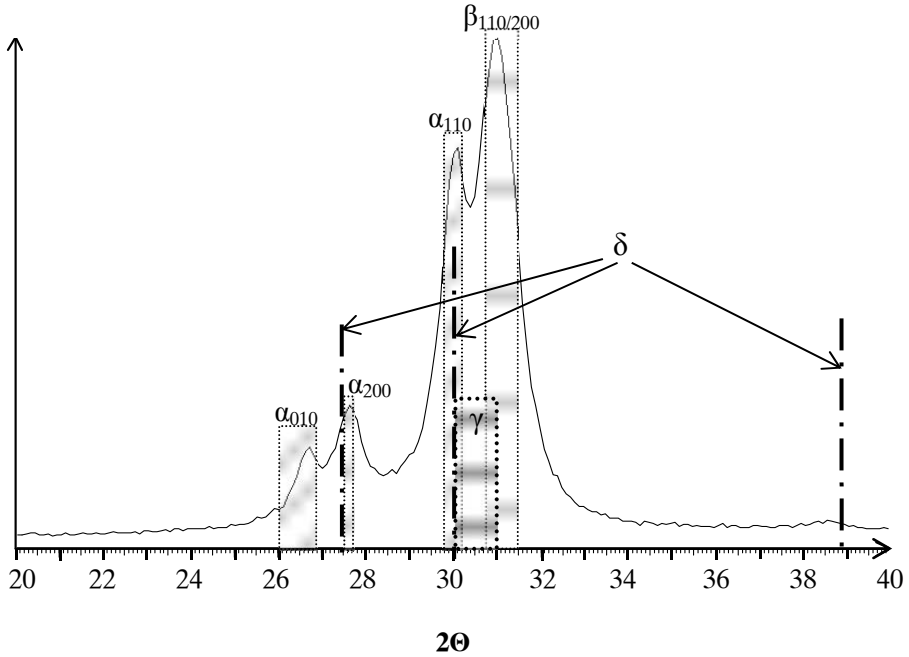

Figure 9 *Representative PVDF X-ray diffractogram, with the main intensity peaks for the four polymorphs indicated. The levels of intensity are arbitrary.*
These 2θ-values are valid for a Cr X-ray source; $\lambda_{Cr} = 0.22897$ *nm*

Two other relatively common methods for characterisation are Fourier transform infrared spectroscopy (FTIR) and differential scanning calorimetry (DSC). In FTIR a number of absorption bands are identified as characteristic for the different phases [34], while in DSC the T_m is expected to be different for the different phases [34-37]. A difficulty with interpreting DSC-results is that T_m is also affected by the chemical interaction between the polymer chains and the thickness of the crystallites; many bonds and a large thickness give a high T_m. Thus T_m can be expected to depend not only on the crystalline phase but also on the conditions of polymerisation and processing [38].

3.4.2 Structure development in PVDF fibres

In an extensive study, Wang *et al.* [35] melt spun PVDF-fibres at MDRs between 20 and 747 from a number of PVDF-grades with different MW. Characterisation by DSC showed different/multiple melting peaks and depending on the MW and MDR, the crystalline melting in the final fibres took place at 165°C, 175°C and/or 192°C. The highest melting peak was interpreted as β phase melting, and it was concluded that β phase formed at a certain minimum spin-line stress or at a certain minimum degree of molecular orientation. Small angle laser light scattering (SALS) was also used to characterise extruded PVDF tapes with three different MWs. This analysis showed that there was a difference in microstructure of the tapes, where the lowest MW sample (Solef 1006) showed a spherulitic structure independent of the MDR, while a higher MW sample (Solef 1010) showed a transformation from the spherulitic structure at low MDR to a "sheaf-and-rodlike" structure at increasing MDR. Again, it was suggested that a transition takes place at a critical stress. No DSC-measurements were reported for the tapes.

Later, Samon *et al.* [31] carried out *in situ* measurements along the spin line using small angle X-ray scattering (SAXS) and XRD and found that early on in the spin-line, shish structures oriented along the fibre axis were formed, however their structure was too defective to cause crystalline XRD reflections. Around the point of solidification, a kebab structure formed perpendicular to the shish and eventually expanded to the point where the shish was locally destroyed. The final morphology was thus not a shish-kebab structure but a lamellar one. The early shish-formation was identified by SAXS and was described not as a crystalline structure but rather a density fluctuation, where the high density domains were expected to have more all-trans conformations, and the lower density domains to contain a high concentration of gauche bonds. Only α phase was formed except at the highest take-up speed where a peak of "extremely low" intensity related to the β phase was present in XRD. It was noted that the spinning rates were lower than in the work from Wang *et al.* [35]. Cold drawing was not done in this study.

Du *et al.* [39] melt spun PVDF towards hard elastic fibres, and showed that the crystalline β phase was induced by cold drawing of the fibres, but that the total degree of crystallinity was unaffected by this procedure. The β-to-α phase ratio was highly dependent on the temperature of

drawing; the optimal temperature was found at 70°C. They also showed that an increase in the deformation rate and/or draw ratio led to an increase in the β-to-α phase ratio.

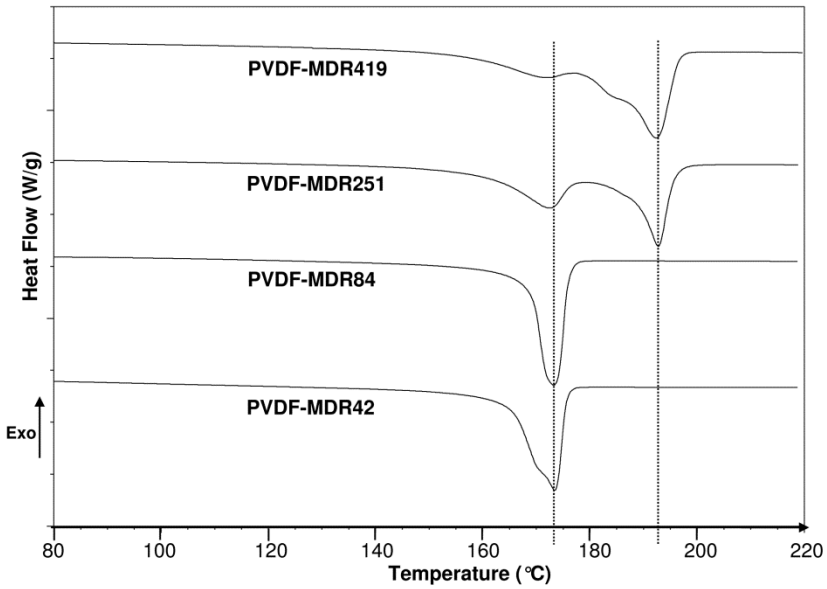

Figure 10 *DSC thermograms of PVDF fibres spun at different MDRs, before cold drawing [from Paper I]*

In our first experiments [Paper I] PVDF monofilament (single fibres) were melt spun from Solef 1010 using different MDRs and λ, as listed in Tables 3 and 4, and characterised by DSC and XRD. Along with the typical melting peak for PVDF around 173°C, a higher temperature melting peak appeared (Fig. 10) for fibres spun at the higher MDRs, consistent with the findings reported by Wang *et al.* [35]. However, the XRD-analysis (Fig. 11) could not support their interpretation of this peak as β phase melting. Instead, our XRD-results show that cold drawing is required for β phase formation, and that the amount of β phase increases with increasing λ (Fig. 12). We concluded that DSC data is not appropriate for crystalline phase identification in PVDF fibres.

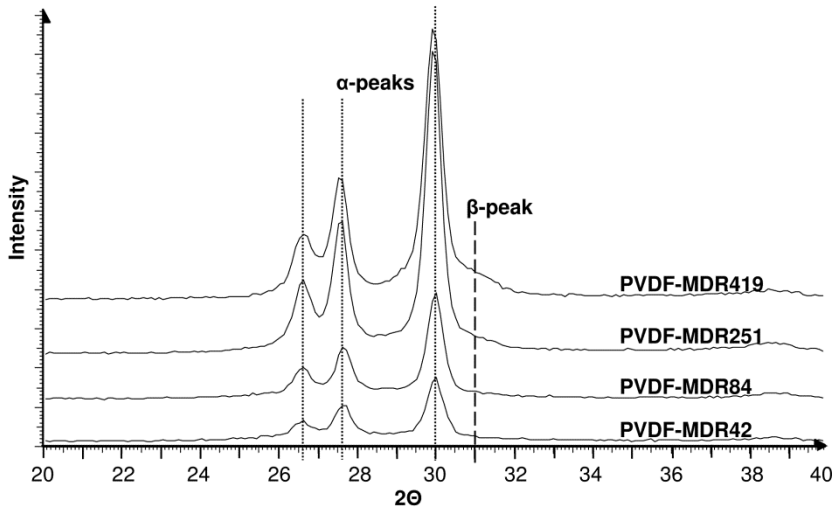

Figure 11 *X-ray diffractograms of PVDF fibres spun at different MDRs, before cold drawing [from Paper I]*

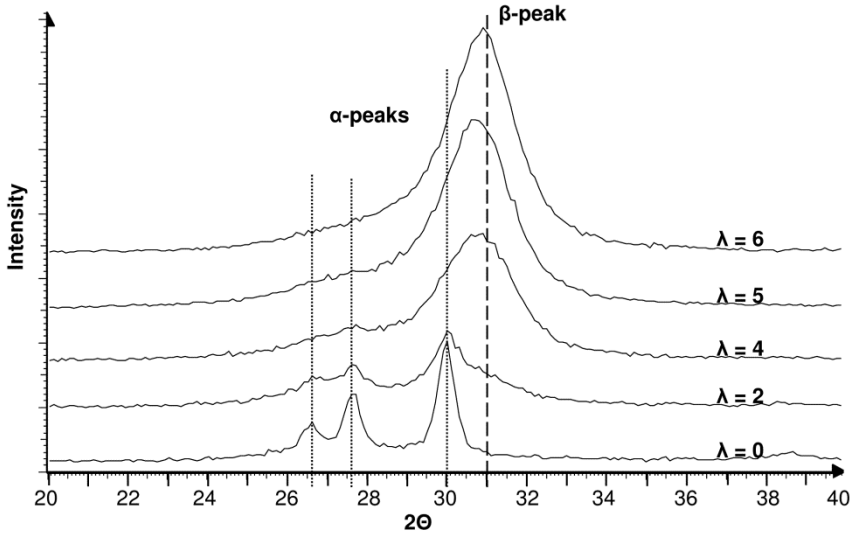

Figure 12 *X-ray diffractograms of PVDF fibres spun with MDR = 42, cold-drawn at different λ [from Paper I]*

PVDF multifilament or yarns (multiple fibres) were subsequently [Paper III] spun at higher spinning velocities (see Tables 3 and 4) in an industrial scale pilot spinning machine. XRD-characterisation confirmed that cold drawing introduces the β phase, and that the degree of β phase increased with increasing λ and, to a lesser extent, with increasing draw rate. The optimum temperature for the drawing rollers was found to be between 70°C and 90°C, consistent with previous reports on PVDF films. It was also concluded that the MDR should be kept low so that the fibres can be drawn to a high extent in the solid state. The multifilament yarns showed a weak tendency towards increasing total degree of crystallinity (X_c) with increasing λ, which was not seen in the monofilament spinning. This was presumably due to the higher deformation rates in the pilot spinning line. In the first bicomponent fibres the β-to-α-phase ratio was lower than in the PVDF yarns with the same *MDR* and λ. This was suggested to be due to the relatively lower $\dot{\varepsilon}_{ss}$ and the higher drawing temperature, which in turn were caused by a decrease in spinnability of the bicomponent fibres compared to the pure PVDF fibres.

The conclusion that cold drawing of the fibres is necessary in order to introduce β is hardly controversial; this was already reported in a number of papers on stretching of PVDF films. These reports also showed that necking is advantageous, and that the draw ratio as well as the draw rate should be as high as possible for maximum α-to-β transformation [40, 41]. Wu *et al.* [42] suggested that the introduction of defects by crystallite breakage during stretching is important for the α-to-β phase transformation to take place. They reported, from *in-situ* SAXS and XRD measurements during cold drawing, that X_c was constant throughout drawing whereas the β-to-α ratio increased with increasing strain. Drawing was suggested to cause the crystalline phase to shear apart and α crystallites to deform into small crystallites, some of which convert into the β form due to rotation of the chain backbone.

Kang *et al.* [43] compared different deformation rates during cold drawing of PVDF fibres; *in-situ* XRD measurements showed that at a high draw rate, there was complete α-to-β transformation and it occurred instantly during necking. At a low draw rate instead, the crystal structure continued to develop during drawing, and the final fibre had a combination of α and β phase crystallinity. *In-situ* SAXS showed that for the final fibre drawn at a high draw rate, the necking introduced

microvoids in the fibre. As the drawing continued, a fibrillar structure (perhaps stacked lamellae) developed in addition to the voids.

Recently, Steinmann *et al.* [44] melt spun PVDF multifilament at high speeds (up to 2500 m/min). The relative degree of β content as well as X_c (by XRD) increased at draw temperatures above 120°C up to the maximum temperature used (140°C). This is in contrast to several studies on PVDF-films which show that drawing temperature exceeding 90°C gives a lower relative β phase content [40, 41, 45, 46]. Steinmann *et al.* proposed that above 120°C, the highly oriented amorphous phase was converted to β phase crystallites. In the same study it was demonstrated, by use of XRD with a heating stage, that in β phase fibres, several phase transformations can occur in the course of heating. At 164°C, β was transformed to α, and at 170°C α was in part melted and in part transformed to γ. Finally, at 184°C, γ phase melted. These transitions were observed both in XRD during heating, and in DSC. It was also noted that the measured degree of crystallinity was much higher from DSC (70-80%) than in XRD (23-27%). This was attributed to the very high degree of order and orientation in the amorphous phase, regarded as a mesophase.

The multiple melting points in DSC-characterisation of PVDF was also studied by Matsuda *et al.* [47], who tied knots on PVDF monofilament and detected an increase in T_m of up to 30°C compared to the unknotted fibres. This is consistent with earlier studies on thermal characterisation of PE fibres, which showed that fibre constraints during measurement may cause a phase transition to take place, thus changing the melting temperatures of the sample [38, 48].

It must be concluded that, although the experimental data from Steinmann *et al.* [44] is very convincing, the thermal transitions in DSC-characterisation of PVDF fibres depend on too many factors for them to be reliable as means for identification of crystalline phases.

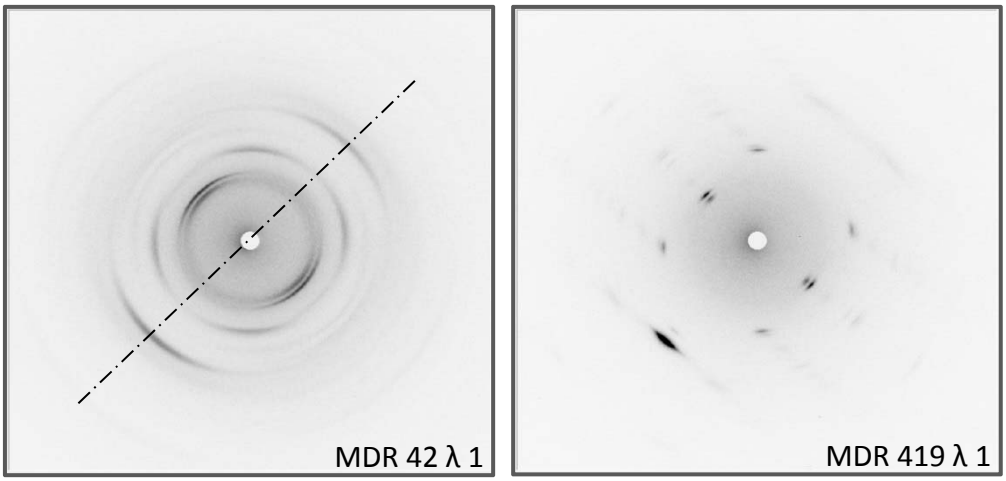

Figure 13 *Representative X-ray images of PVDF fibres spun at low and high MDRs as described in Paper I. The dotted line indicates the direction of the fibre axis.*

As our equipment does not provide means to quantify the degree of crystallinity or peak width from our X-ray diffractograms, supplementary XRD-characterisation[1] was recently carried out on our first fibres [Paper I] using a single-crystal diffractometer (Fig. 13) and the results are given in Table 5. The average values of the crystallite sizes (in the direction parallel to the fibre axis) were calculated from the half-width of intensity peaks. The relative amounts of α and β crystallites were derived from the peak areas. The results confirm that there is no β phase present in fibres before cold drawing, and that crystallites are thicker in the fibres spun at MDR 251 and 419, compared to MDR 42. The results also confirm that the degree of crystallinity is higher in the fibres spun at high MDRs, although all the numbers for X_c are much lower in XRD (24-48%) compared to DSC (60-90%).

[1] The supplementary XRD-analysis was carried out at Aachen RWTH, Germany. A single-crystal diffractometer STOE IPDS II was equipped with an image plate for digital readout and a special holder for fibres. The X-ray source was Mo-K_α. Image processing was carried out using in-house developed software.

Table 5 *Summary of results from supplementary XRD-measurements on PVDF monofilaments spun as in [Paper I]*

Spinning parameters	Degree of crystallinity (%)	α fraction (%)	β fraction (%)	Crystal size α (nm)	Crystal size β (nm)
MDR = 42 λ = 1	27	-	-	-	-
MDR = 42 λ = 6	24	0	100	n/a	11
MDR = 251 λ = 1	35	99	1	18	n/a
MDR = 251 λ = 2	48	23	77	14	24
MDR = 419 λ = 1	39	99	1	20	n/a

n/a: not applicable

3.5 Adding nanoparticles to control the morphology

There exists currently considerable interest in adding nanoparticles to commodity polymers as means to increase their application range [49]. Specifically, carbon nanotubes (CNT) are added to PVDF in order to induce electrical conductivity and to enhance the β-to-α phase ratio. The percolation threshold, the concentration at which conductivity abruptly increases, is reported at 0.07 wt% [50], 0.19 wt% [51] and at 0.2 wt% [52], depending on the type of CNT and procedure for mixing.

Enhanced β phase content, or β to α phase ratio, has been observed at CNT-concentrations from 0.001 to 2 wt% [50, 53, 54]. The standard procedure for preparation of a CNT/PVDF composite includes dissolving PVDF and dispersing CNT in a suitable solvent, then using stirring and ultrasonication in order to improve the particle dispersion. Yu *et al.* [54] compared composites prepared using this route, to composites prepared without ultrasonication, and found a significantly larger amount of β phase in ultrasonicated samples. They suggested that this is due to the ultrasonication process providing a sufficient amount of energy to transform the (α) TGTG'- type chain conformations into (β) all-trans conformations, and that the all-trans conformation chains will be tightly bound to the CNT surface and act as nucleating sites for β phase

crystallites. The all-trans conformed chains close to the CNT surface are unlikely to transform to TGTG'-conformation, due to their strong bounds to the highly confining CNTs. The positive effect of CNT was recently confirmed by Guo *et al.* [55], who showed that the incorporation of 0.01 wt% double wall nanotubes (DWNT) in melt spun PVDF fibres could enhance the α to β phase transformation during cold drawing. The DWNT composite fibres also exhibited a higher total degree of crystallinity compared to PVDF fibres.

On the other hand, Almasri *et al.* [51] used the same procedure including ultrasonication, but their composite films had no β phase crystals. Their CNT/PVDF composites had a lower total degree of crystallinity and a higher crystallisation temperature (T_c) compared to pure PVDF. The authors suggested that these factors indicate a high nucleation ability of the CNTs, combined with a low crystallisation rate due to restriction of the polymer chains by the CNTs. The difficulty in inducing phase transformation by CNT-addition was predicted in a recent computational study: the results indicated that for short PVDF-segments, the α conformation was preferred both in the presence and in the absence of a CNT and that, based on the calculated binding energy, the PVDF chains are more likely to bind to each other than to a CNT [56].

In paper II, we showed that the addition of 0.01wt% DWNT could introduce β phase without cold drawing. This only happened if the DWNT were introduced by a mixing process that included a solvent and ultrasonication; the addition of DWNT directly in the polymer melt did not help in introducing β phase crystallites.

It may be noted that adding CNT to PVDF is reported to enhance the piezoelectric effect in ways that are not related to β phase enhancement. For example, CNT/poly(vinylidene fluoride-trifluoroethylene (P(VDF-TrFE)) composite nanofibres were produced by electrospinning, and the addition of 0.05 wt% of CNT caused an increase in the strain-sensing ability (output voltage across the sensor) by 35 times. The results were attributed to the presence of aligned "piezoelectric CNT" [57].

Others have reported that by incorporating CNT in PVDF, the dielectric constant can increase dramatically [52, 58] compared to the pure PVDF. This is explained as a formation of a capacitor network in the composite, and may result in enhanced polarisation and piezoelectric properties.

3.6 Summary part I

Thus to summarise, our results indicate that in response to the first research question (see section 1.2 Aim):

- Cold drawing of the PVDF-fibres is necessary to introduce β phase, and the draw ratio should be as high as possible
- Cold drawing is preferably carried out at a temperature between 70°C and 90°C
- Adding CNT may be helpful under specific processing conditions

4. Towards piezoelectric fibres

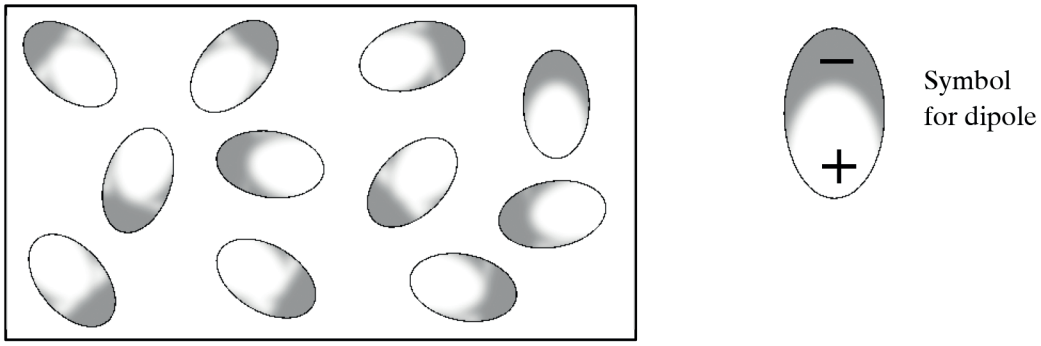

Figure 14 *Schematic illustration of randomly distributed dipoles in an amorphous matrix*

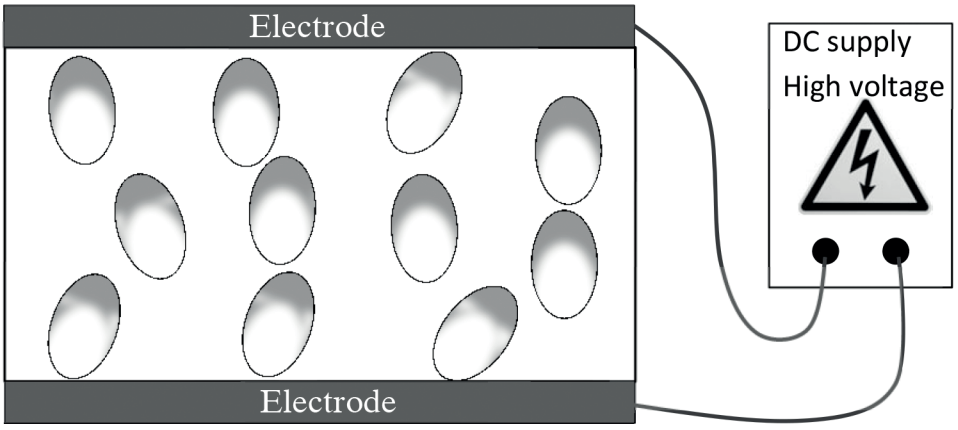

Figure 15 *Schematic illustration of dipole alignment during poling*

In fibres melt spun at the right conditions, there will be a certain degree of polar β phase crystals present. These polar crystals can be expected to be randomly distributed in the amorphous phase (Fig. 14), and for the PVDF to be polarised on a macroscopic level the dipoles must be coherently oriented. This orientation, or polarisation, is introduced by applying an electric field of sufficient strength across the sample (as in Fig. 15), a process known as poling. After poling, applying an external force to the polymer will cause a change in the charge density, which appears as a change in the electric field across the sample and can be measured as an electric voltage. The piezo- and pyroelectric coefficients are linear functions of the remanent polarisation. Prior to poling, electrodes must be applied on one or two sides of the piezoelectric

medium. While applying electrodes to a film can be done by simply metallising its two sides, electroding of fibres is seemingly more difficult and can be done in a number of ways.

4.1 Electroding of thin fibres

4.1.1 Ceramic fibres

Ceramic piezoelectric fibres are commercially available and used as sensors, actuators and for energy harvesting. In current practice they are made from lead-zirconate-titanate (PZT) and embedded in for example a polymer-based matrix for mechanical support. Electrodes can then be applied by adding an electrically conductive component to both surfaces (as in Fig. 16 b) [59, 60]. Ceramic fibres have also been produced with a coaxial metal core working as an inner electrode, and were embedded in an electrically conductive polymer matrix working as a common outer electrode (Fig. 16 c) [61]. In a third example, ceramic fibres may employ interdigitated electrodes (Fig. 16 e); arrays of narrow conductors applied on the fibre surfaces, perpendicular to the fibre direction [62].

4.1.2 Electrospun PVDF fibres

In electrospinning, a polymer solution is ejected and stretched under the influence of a strong electric field. The solvent evaporates in the process and a nonwoven mat of fibres with diameters in the nano-scale is produced. Electrospinning of PVDF is reported to introduce both β phase [63-65] and electrical polarisation [66, 67]. PVDF nanofibres have been spun directly onto two separated electrodes similar to Figure 16 f [65], or the mats have been electroded according to Figure 16 a by adding a conductive tape or similar to each side [67].

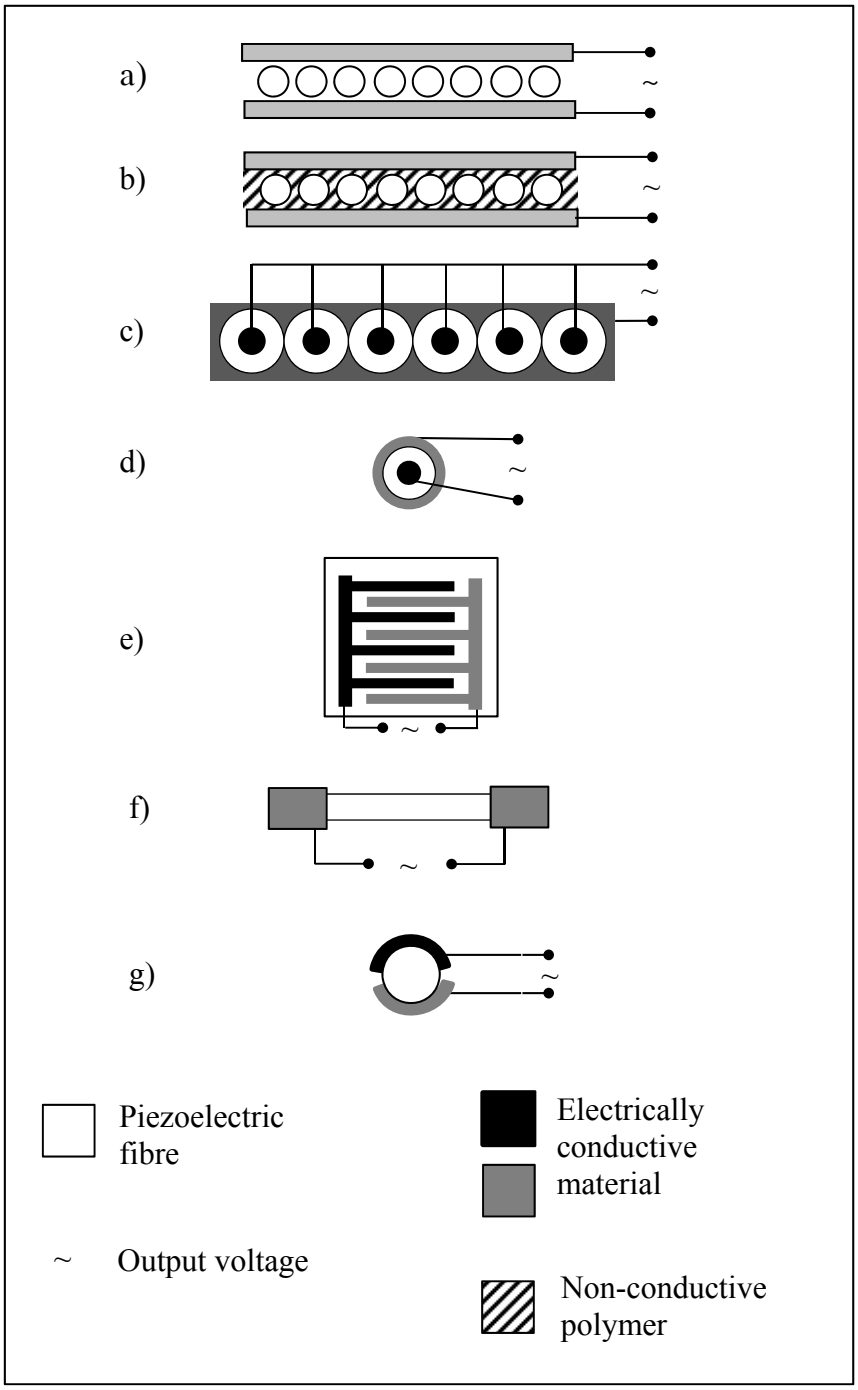

Figure 16 *Electroding schemes used with piezoelectric fibres:*
a) and b) laminated surface electrodes (cross-section)
c) bicomponent fibres with a common outer electrode (cross-section)
d) tricomponent fibre (cross-section)
e) interdigitated electrodes (top view)
f) fibre-end electrodes (top view)
g) surface electrodes (cross-section)

4.1.3 Melt spun piezoelectric polymer fibres

Melt spun piezoelectric fibres are relatively unexplored; to the best of the author's knowledge there are only a few very recent publications on the matter. Egusa *et al.* [68] presented a hollow 5-layer composite fibre where the piezoelectric component was P(VDF-TrFE) placed in between two layers of carbon-loaded PC (similar to the scheme in Fig. 16 d). The center and outer layer were PC with thin indium electrodes placed in parallell with the fibre axis. This fibre was in fact not melt spun but thermally drawn from a preform. The fibre showed both direct and reverse piezoelectric response.

Walter *et al.* [69] demonstrated the direct piezoelectric effect in melt spun PVDF monofilament. The fibres were embedded in an epoxy matrix with the fibre axes aligned parallel to the composite surface. The composite structure was poled between two parallel metallic electrodes, and for piezoelectric measurements, copper films were attached as electrodes to the composite surfaces (as in Fig. 16 b).

Ito *et al.* [70] reported a strong piezoelectric effect from a PLLA-fibre. The fibre was wound and annealed to form a coil; this coil was then placed around the arm of a test subject, and the response signal from the fibre was used to monitor and visualise the arm motions of the subject. The electrodes were placed on the surface of the fibre parallell to its axis, according to Figure 16 g. Two noteable differences in PLLA compared to PVDF are that PLLA does not require poling, and that it mainly possesses shear piezoelectricity.

The electroding options shown in Figures 16 a, e, f and g would not practically work with PVDF fibres, or more specifically, in the poling of PVDF fibres. Due to the short distance between electrodes in Figure 16 a, e and g there would be flashover between the electrodes during poling, and in contrast, the long distance between the electrodes in Figure 16 f would necessitate unrealistically high poling voltages. The addition of an insulating polymer layer, as in Figure 16 b, also presents difficulties as this polymer must have a dielectric strength close to that of PVDF; Walter *et al.* [69] did report difficulties in applying high voltages.

4.2 Piezoelectric bicomponent fibres

For ease of fabrication it is preferred that the electrodes are manufactured as an integrated part of the spinning process. A convenient way is to use bicomponent spinning with a core and sheath configuration, where the core is electrically conductive and can act as an inner electrode (see Fig. 17). The outer electrode may then be added according to Figure 16 c or d. Adding CB to a polymer matrix is by now an established method to produce an electrically conductive composite. At the percolation threshold the CB forms a percolating network through the polymer matrix, resulting in electrical conductivity. The compound is regarded as conductive if volume conductivity σ_v exceeds 10^{-3} S/cm. The final electrical properties of the composite depend on several factors including compounding and the particular type of the CB [71, 72]. The evaluation of such factors is beyond the scope of this thesis.

Spinning fibres with an electrically conductive core was based on previous research in our group, of which a brief summary is given here. Hagström [73] studied melt spinning of CB/PP composites. The percolation threshold for extruded strands, drawn only by gravitational force, was at 1.8 wt% CB. The shear viscosity of the CB/PP compound clearly increased already at 2 wt% CB, and at higher loadings the melt became highly elastic which is inappropriate for melt spinning. At CB loadings of 8 wt% and above melt spinning could not be done due to spin line break. This was because adding CB to a polymer melt restrains the chain mobility of the polymer, resulting in increased melt viscosity and reduced spinnability. Spinning the lower concentration compounds was associated with a decreasing conductivity at increasing melt draw ratios, probably due to a loss of contact between the conductive particles. Similar results were presented by Stråat *et al.* [74] who melt-spun monofilament from a CB/PE compound with CB concentrations up to 7 wt%.

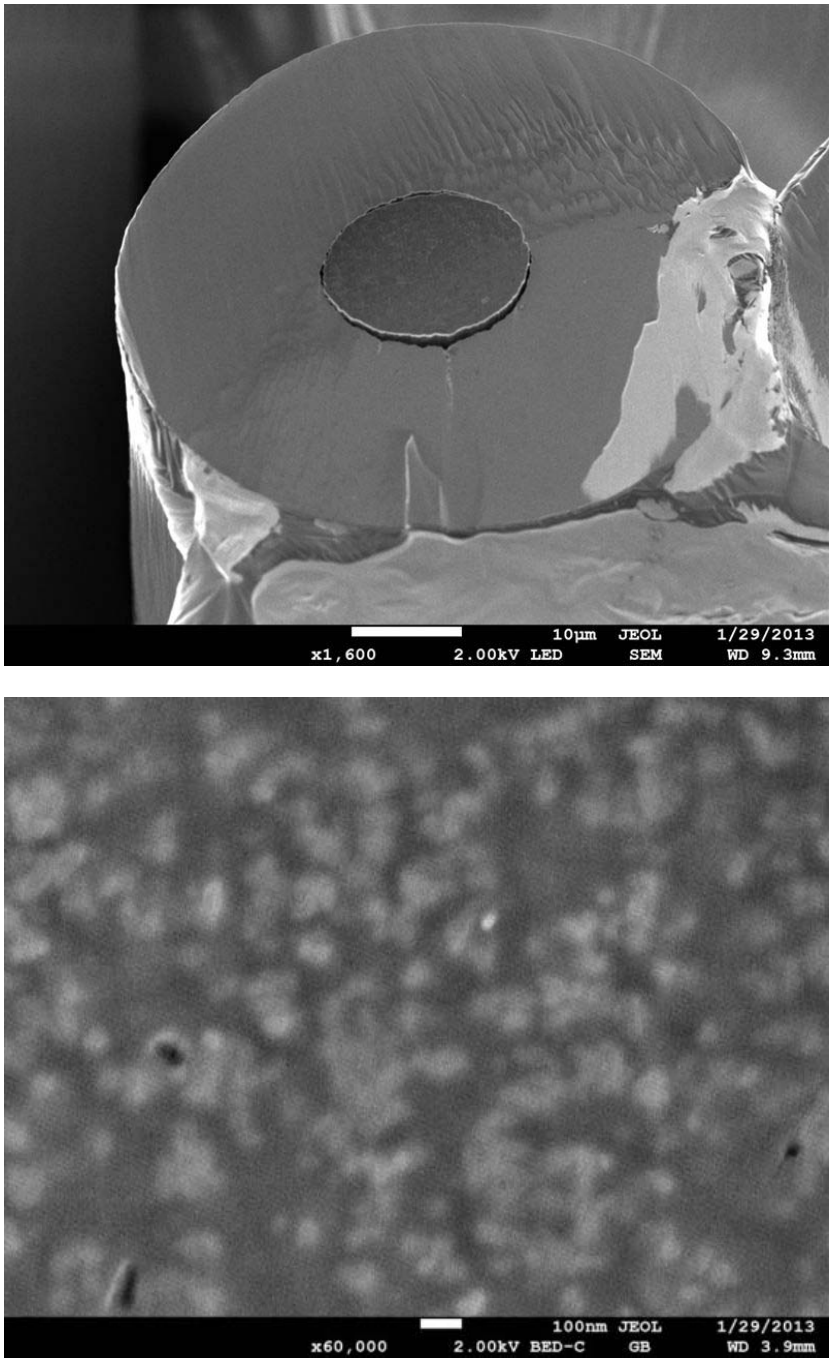

Figure 17 *SEM images of a bicomponent fibre cross-section. The fibres have a PVDF sheath and CB/HDPE core with 10 wt% CB, as described in [Paper V].*
Top: bicomponent fibre cross-section. Scale bar is 10µm.
Bottom: cross-section of the fibre core; the white spots are CB. Scale bar is 100 nm.

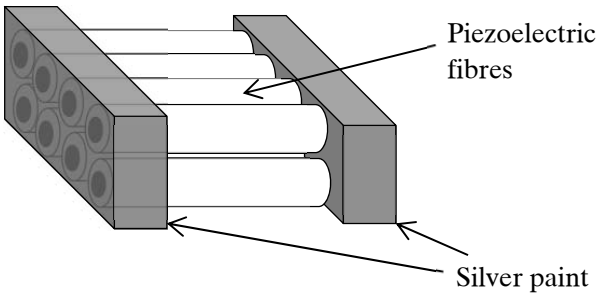

Figure 18 *Illustration of the electrical connection to the inner electrodes*

Stråât *et al.* [75] went on to spin fibres with higher concentrations of CB by placing the compound in the core of a bicomponent fibre with a highly spinnable polymer as sheath material. The spinnability improved with increasing volumetric sheath/core ratio and became poorer with a lower viscosity sheath material. This was attributed to the fact that the sheath material bears a major share of the spin line force. The drawing process involved in fibre spinning, especially the solid state drawing, still caused a decrease in conductivity at increasing draw ratios. By reheating the fibres above the melting point of the core compound electrical conductivity could be restored or at least improved. This was explained by diffusion of the filler in the polymer resulting in increasing agglomeration of CB particles and diminishing separation distances between CB domains, resulting in a restored conductive network [72, 76].

Very recently, bicomponent spinning of PVDF with a conductive core was reported by Ferreira *et al.* [77] who extruded monofilament with a CB/PP core, and by Glauß *et al.* [78] who melt-spun multifilament with a CNT/PP core. Neither of these studies reports any poling or piezoelectric characterisation of the fibres.

In our first experiments on spinning β phase PVDF yarns with an integrated core [Paper III] a CB/PP compound with 8.5 wt% was used as core material. The core conductivity was measured as the volume conductivity σ_v, defined as:

$$\sigma_v = I\rho l^2/(Um) \qquad \text{(Eq. 1)}$$

where U is the measured voltage, m is the mass of the core material, I is the measured current, ρ is the density of the core material and l is the

length of the sample between the silver paint contacts. For conductivity measurements, poling and piezoelectric characterisation, the core electrodes were contacted by immersing the cut fibre ends in silver paint (schematically illustrated in Fig. 18).

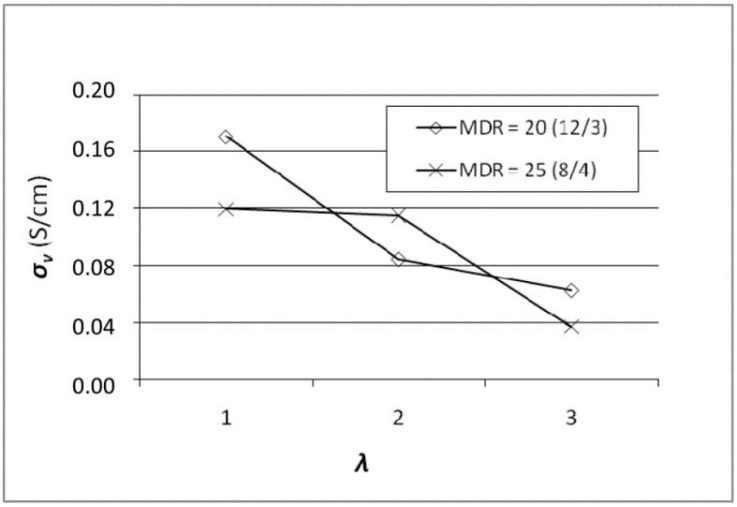

Figure 19 *Core conductivity σ_v, of bicomponent yarns as a function of λ, with different sheath/core volume ratios [from Paper III]. The core was 8.5 wt% CB in PP.*

The σ_v decreased significantly after the cold drawing necessary to introduce β phase crystallinity (Fig. 19). As heat treatment at a temperature above the T_m for PP (around 165°C) was expected to destroy the β phase, the core polymer had to be replaced by one with a lower T_m. Two different PE-based polymers were evaluated for the core compound [Paper IV]; CoPE is an ethylene-octene copolymer elastomer with T_m = 80°C, and HDPE is a high density PE with T_m = 129°C. Both were mixed with 10 wt% CB. After heat treatment, the HDPE compound showed an expected increase in conductivity, whereas the CoPE compound showed a decrease in conductivity (Fig. 20). This was assumed to be due to a poor final distribution of CB-particles in the CoPE matrix. The relatively higher conductivity in the HDPE matrix may also be attributed to the high degree of crystallinity in this polymer, promoting a two phase system where CB particles reside in the amorphous phase. As the electrodes should have as high conductivity as possible, HDPE was selected for the core compound in the continued experiments.

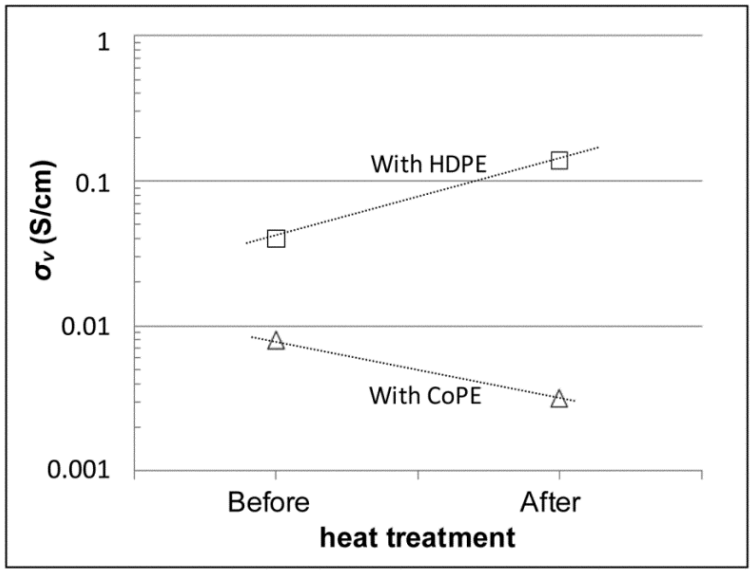

Figure 20 *Core conductivity σ_v, of bicomponent yarns with two different core polymers and 10 wt% CB, before and after heat treatment [from Paper IV]. The yarns were spun at MDR = 30 and λ = 4.5 (for CoPE yarns) and at MDR = 23 and λ = 4 (for HDPE yarns) respectively.*

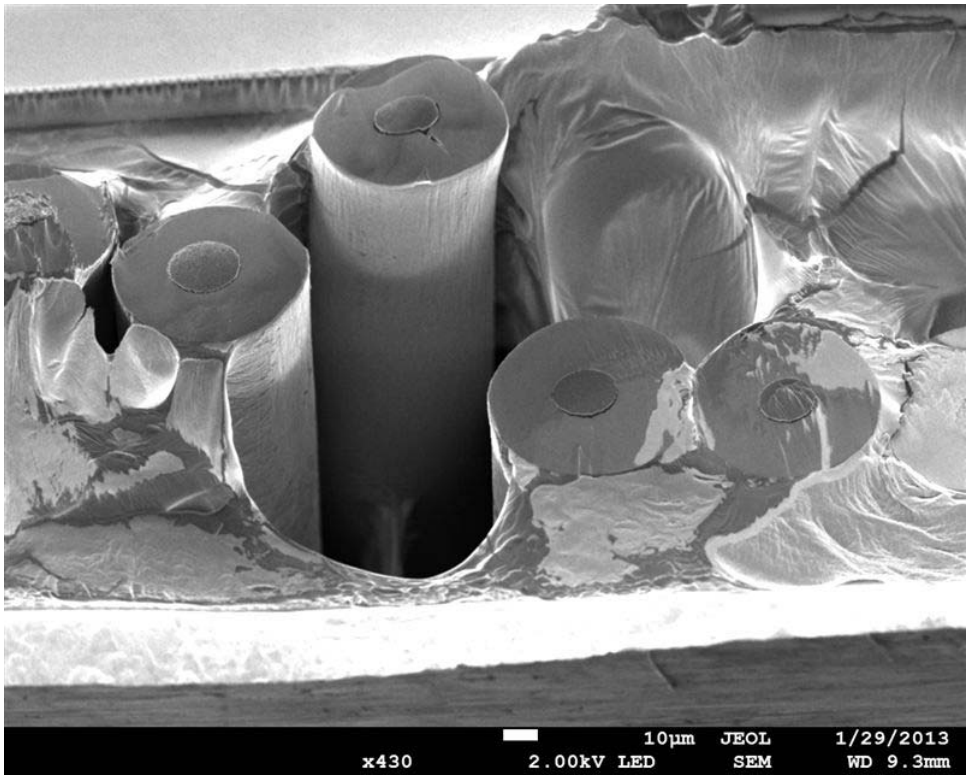

Figure 21 *SEM image of cross-sections of the bicomponent yarns with 10% CB/HDPE as core, embedded in silver paint. Scale bar is 10µm.*

To enhance spinnability, the sheath PVDF (Solef 1008) was replaced with Solef 1006 which has lower MW and viscosity, and bicomponent β phase PVDF yarns were successfully spun using a 10% CB/HDPE compound as the core material.

Figure 17 and 21 show scanning electron microscopy (SEM) images[2] of these yarns embedded in silver paint. The cross-sections were cut and ion-polished prior to imaging. The core and sheath materials are well separated, and the CB particles seem to be rather well distributed within the core. Some defects can be noted; there is a variation in the relative core/sheath volume ratios and small cracks are visible in the PVDF sheath.

4.3 Poling

4.3.1 Contact poling and thermal poling

In the conventional contact poling method for PVDF films, electrodes are applied to both surfaces (as in Fig. 15) and a high voltage V is connected to the electrodes for a certain period of time t. Contact poling is generally done at an elevated temperature T, and may then be referred to as thermal poling. For efficient polarisation, the electric field E ($E = V/z$, where z is the PVDF thickness) should be close to the dielectric strength which depends on the PVDF thickness. According to the PVDF data sheet [11], the dielectric strength is 100 MV/m for a 25 μm thick film and 50 MV/m for a 200 μm thick film.

There are a number of studies on poling of PVDF films and although they are not in full agreement, their results give valuable guidelines. Typically, a PVDF film with metallised surfaces is polarised by an electric field between 40-200 MV/m at an elevated temperature of 30-150°C [79-82]. Poling times between 0.1 and 1300 min, after which (in most cases) the electric field is maintained during cooling, have been studied. Day *et al.* [79] reported that the final pyroelectric response p in PVDF films increased steadily with both V and T, whereas increasing t also had a positive effect but was the least important factor.

---

[2] SEM images were obtained using a field-emission gun SEM (FEG-SEM) JSM 7800 F from Jeol, Japan, in back-scattering mode. Ion polishing was carried out with a 693 Gatan, USA.

Blevin [80] found that at a certain poling voltage, p was hardly affected by T provided that t was long enough. It was suggested that the poling mechanisms were independent of temperature. DeRossi *et al.* [81] reported that at a certain poling time, increasing T or V gave a higher p.

Contact poling can also be carried out at room temperature, in which case the electric field should be in excess of 200 MV/m [82, 83]. A practical difficulty in poling of PVDF is due to the relatively low dielectric strength of air; approximately 3 MV/m. Thus care must be taken during experimental setup to avoid flashover or arcing between the electrodes. One solution is to place the electroded film in vacuum or in insulating oil. Wang & von Seggern [83] placed an insulating rubber ring around the electrode area of a film and managed to apply up to 900 MV/m without flashover, for a short period of time.

4.3.2 Corona poling

In corona poling one or several needle electrodes are placed at a distance of a few centimetres from one side of the film or fibre (Fig. 22), while the other is electroded and at ground potential. When a high voltage is applied to the needle, corona discharge from the needle tip will follow, generating ions in the surrounding air. The ions transfer their charge to the exposed film surface and an electric field develops between the charged surface and the opposite grounded surface, orienting the molecular dipoles. With this method higher voltages can be applied than in contact poling [84]. Corona poling is also attractive as it provides an opportunity for poling as a continuous process.

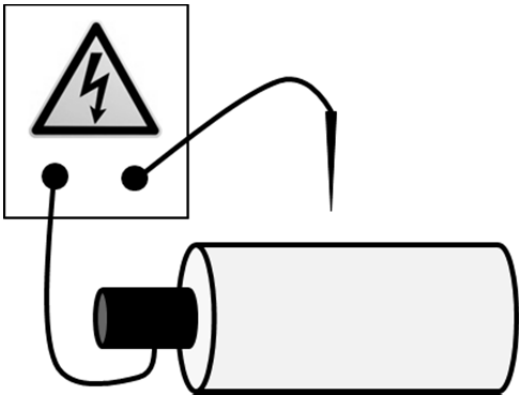

Figure 22 *Principle for corona poling of a bicomponent fibre (fibre size is exaggerated)*

At a certain minimum electric field strength, in the order of 200 MV/m, polarisation has been reported to occur in less than 1 s at room temperature [85]. At lower electric fields, when applying corona poling for 30 min, d_{31} increases with increasing poling field E. At E above 160 MV/m α phase is transformed to β [86, 87].

4.3.3 Polarisation mechanisms

In his first report on piezoelectric PVDF, Kawai [3] demonstrated that if PVDF was adequately polarised, the polarisation and accompanying piezoelectric effect were stable over a long period of time. The piezoelectricity was suggested to be due to the permanent orientation of dipoles in the molecular chains, perpendicular to the film surface [88]. In the next few years there was some debate on whether the main physical mechanism was the oriented dipoles, charge trapping, or a combination of both [89].

While the details are still open for discussion, there seems now to be a general agreement that the orientation of dipoles, induced by an electric field as described in section 4, is the main factor [90]. This is supported by several experimental studies showing that the remanent polarisation and piezoelectric activity increase with increasing β phase content [91-93]. In addition, a shift in orientation of CF_2-dipoles along an electric field has been observed by XRD [86, 94] and by FTIR [89, 95]. According to one model of polarisation the orientation proceeds through chain rotations in steps of 60°, where small domains (a few chains) in a crystal rotate sequentially resulting in a line of advancing polarisation. As chain mobility is highly restricted within a crystallite, rotation must be initiated at a boundary surface. The process is accompanied by a small distortion of the lattice [96].

Poling at higher temperatures reduces the coercive field E_c (the field at which dipoles are reoriented)[90, 97], while the polarisability of PVDF is very low at temperatures around T_g [97, 98]. The enhanced polarisation at higher temperatures is explained to be a result of easier chain rotation and a higher mobility of charge carriers. Because the rotation of each segment can occur at a certain threshold E, varying degrees of crystal perfection lead to a distribution of the E_c [92]. The degree of orientation is also affected by crystallite size and degree of crystallinity [97].

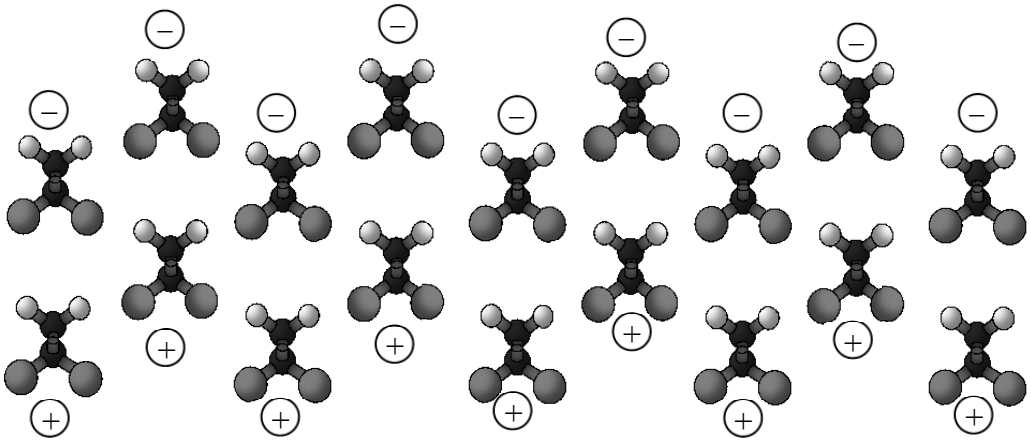

Figure 23 *Schematic cross-section of a polar PVDF crystallite with trapped charges at the dipole ends, stabilising the dipoles' positions*

Experimentally, polarisation (C/m^2) is commonly measured as a function of an applied alternating electric field. It is reported that the polarisation of PVDF is unstable in the sense that it gradually increases as the number of poling cycles increase [95, 99]. Time dependence is also observed and polarisation seems to include two processes, where the first is instantaneous and the other is relatively slow. The actual elapsed times for these processes vary depending on the poling parameters as well as the prehistory of the PVDF sample, however the degree of remanent polarisation is equal to that introduced in the slower polarisation process. Several explanations are proposed:

1) The time dependence is due to a variation in the initial orientation of the dipoles, so that some of them require more time to orient themselves along the field [100].

2) The slow process is due to a phase transition from α to δ [101].

3) The dipoles are oriented instantly, and then charges are injected and trapped by dipoles at the surfaces of the crystallites (illustrated in Fig. 23). The free charges are necessary for stabilisation, and if poling is interrupted before the required charge injection can take place, the dipoles will flip back [101, 102].

The theory of injected charges being necessary for stable poling is supported by an experiment where a P(VDF-TrFE) film was poled with thin insulating PET films blocking the electrodes. The results showed that the polarisation in this sample was the same as in a film poled without insulator, as long as an electric field was applied. However when the voltage was removed, the film with insulating electrodes showed no remanent polarisation, whereas the other film did. The electric field was applied for 50 ms [103]. On the other hand, successful poling (after 30 min) of PVDF monofilament embedded in insulating epoxy is also reported [69].

4.3.4 Piezoelectric characterisation

For characterisation of piezoelectric properties, two piezo coefficients are used. The strain constants – or the "d" coefficients – relate the mechanical strain produced to the applied electric field. The voltage constants – or the "g" coefficients – relate the electric field produced to the mechanical stress applied. These constants are given with two subscripts, where the first subscript refers to the electrical axis and the second one refers to the mechanical axis. The axis denoted 3, or the polar axis, is taken parallel to the direction of polarisation within the specimen (indicated by the arrow P in Fig. 24).

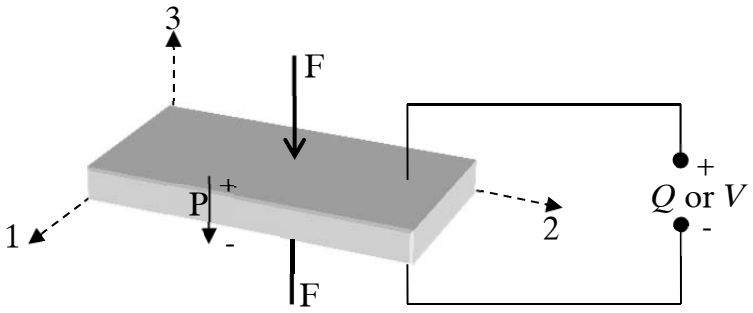

Figure 24 *Numerical classification of axes related to piezoelectric characterisation*

Its direction is thus established during poling. As an example, the coefficient d_{33} gives the relation between the strain developed under an applied electric field and the magnitude of the electric field, in m/V. The 33 subscript indicates that the electric field and the mechanical stress are both along the polarisation axis, as illustrated in Figure 24 [60].

4.3.5 Piezoelectric characterisation of bicomponent fibres

For our first piezoelectric characterisation [Paper IV], a number of fibres were embedded in a conductive CB/CoPE compound working as a common outer electrode (as in Fig. 16 c), and the core electrodes were contacted by silver paint. The fibres were thermally poled at $T = 100°C$ and $V = 1$ kV ($E = 56$ MV/m). This was clearly sufficient to polarise the fibres, as could be verified by measuring an output voltage corresponding to a dynamic compression of the fibres (Fig. 25).

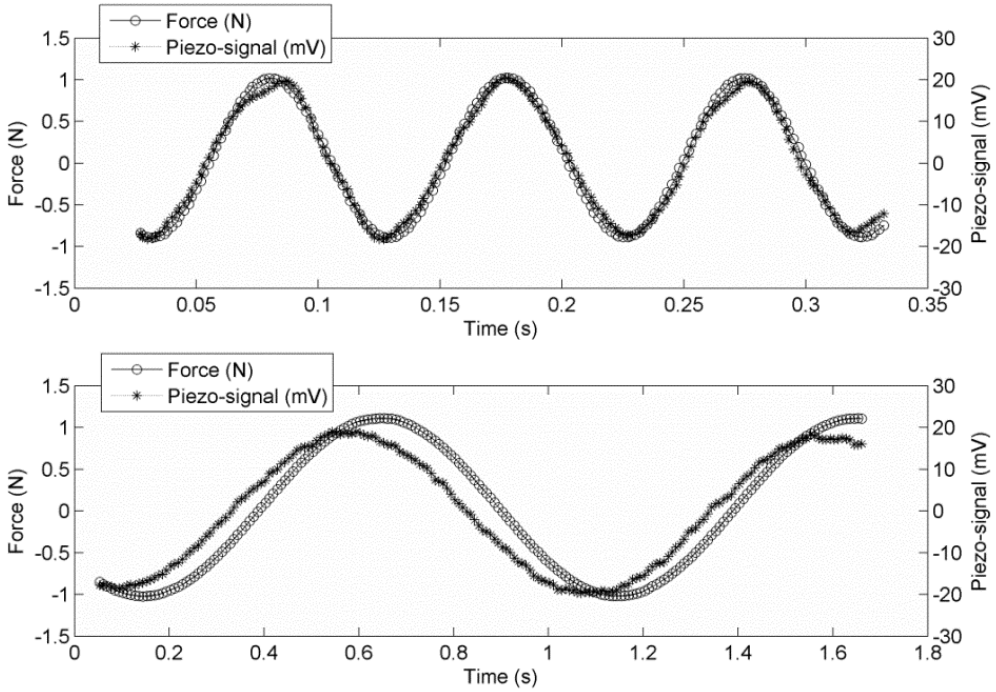

Figure 25 *Example of the resulting force and voltage output from the piezoelectric fibres as a function of time during an oscillating compression at 10 Hz (top) and 1 Hz (bottom) [Paper IV]*

The fibres were further characterised under dynamic stretching along the fibre axis [Paper V], and showed orders of magnitude higher voltage outputs (Fig. 26) compared to the characterisation under compression.

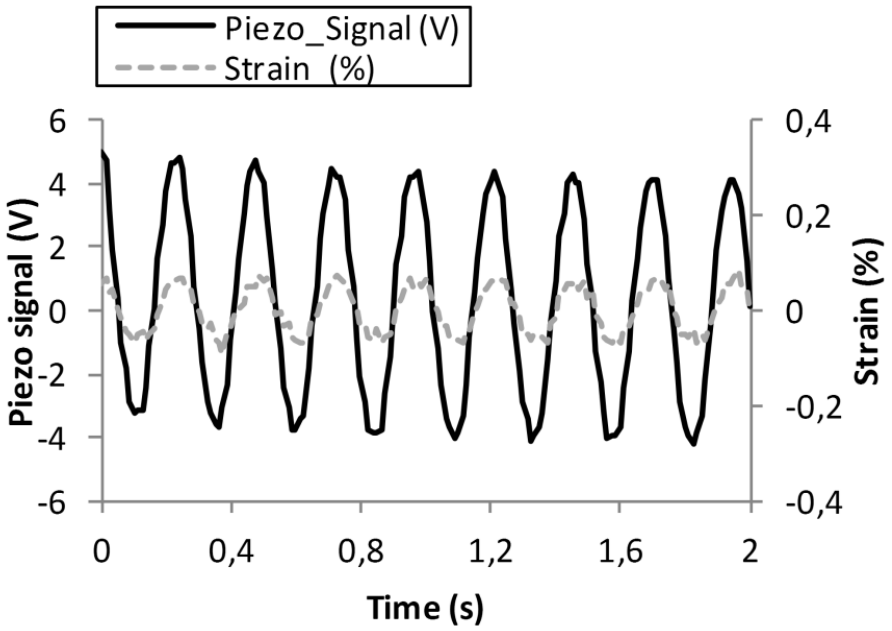

Figure 26 *Piezoelectric signal and strain as a function of time for a yarn (24 fibres) during dynamic stretching at 4 Hz [Paper V]*

This should be due to the direction of the electrical axis (Fig. 27) in relation to the direction of the mechanical deformation. When compressing the bicomponent fibre, the deformation parallel to the applied force is compression, while in the orthogonal direction there is expansion. Thus the charge effects in these two regions will be counteracting. On the other hand, if the fibre is stretched along its fibre axis, the deformation should be well distributed radially, and the resulting charge output is higher (illustrated in Fig. 28).

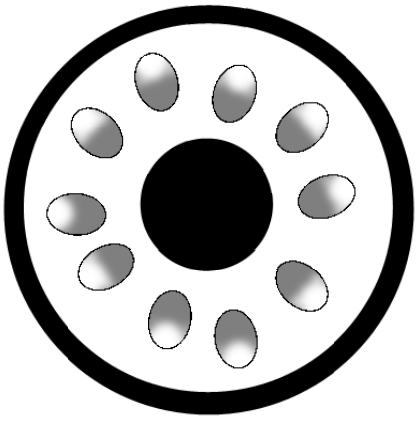

Figure 27 *Expected orientations of dipoles after poling*

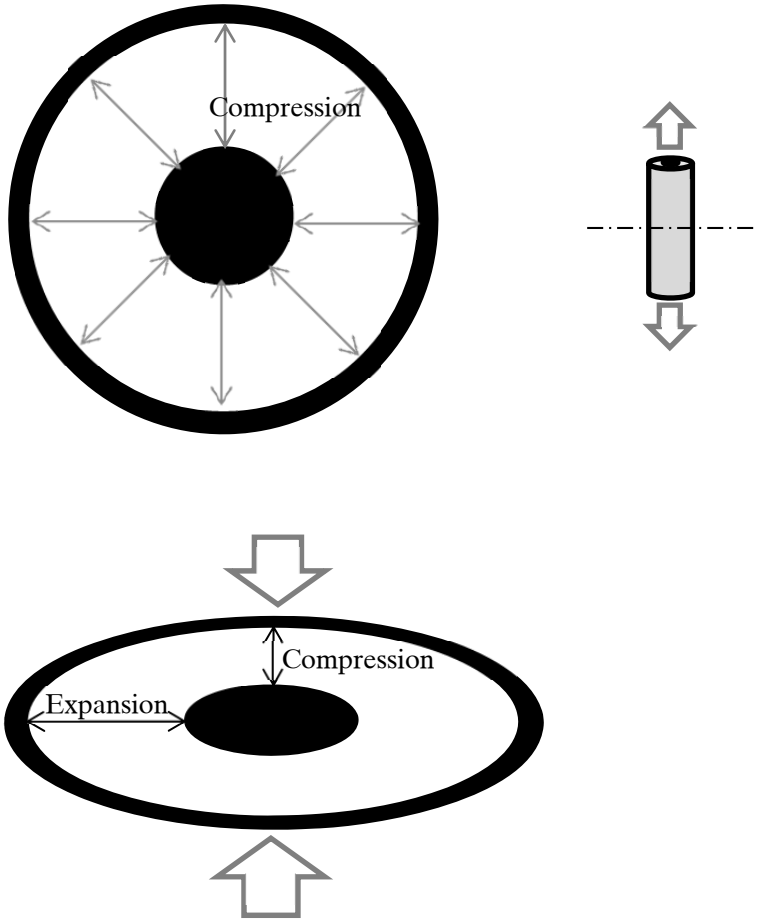

Figure 28 *Mechanical deformation as a result of stretching (top) and compression (bottom)*

4.3.6 Poling of PVDF bicomponent fibres

In Paper V, contact poling was carried out with varying T, t and V, and the poling efficiency was evaluated from the resulting piezoelectric effect. We found that for maximum piezoelectric output, T should be 60°C and V should be as high as possible. The poling time did not have a strong influence on the result. The poling maximum at 60°C seems to be consistent with a general relaxation in PVDF-chains around this temperature, reported as a mechanical relaxation by Steinmann *et al.* [44], as a dielectric relaxation in the datasheet [11], and as a current peak in thermally stimulated discharge measurements by Eliasson [104]. The highest electric field used here, 101 MV/m, corresponds well with the dielectric strength for a PVDF film of the same thickness [11].

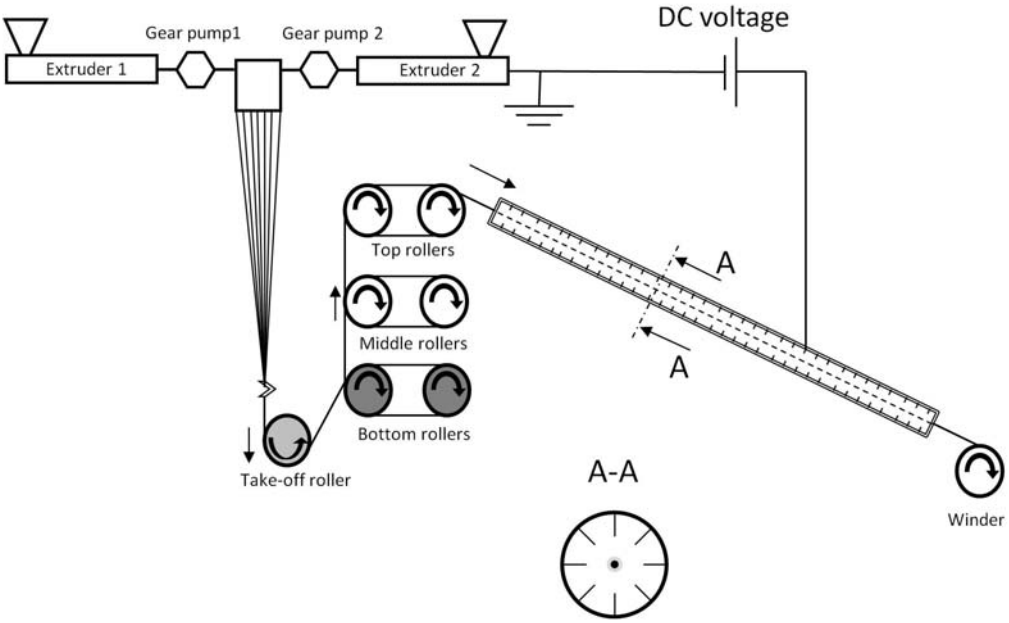

Figure 29 *Illustration of the spinning machine with in-line corona poling*

Room temperature corona poling at different *t* and *V* showed the same trend; *V* should be as high as possible and *t* can be very short. The piezoelectric effect from corona-poled fibres was generally lower than that from fibres contact-poled at higher temperatures, but higher than in fibres that were contact-poled at the lowest *T* (40°C). We also showed [Paper V] that room temperature corona poling could be carried out in a dynamic mode, with the fibres passing through a "poling zone". This was recently developed by us towards equipment for in-line poling, where the bicomponent fibres are poled within the spinning process. As illustrated in Figure 29, in-line poling can be carried out by winding the fibre through a long tube with a large number of corona needles pointing inwards. In this set-up, the core is electrically grounded via the spinning machine.

4.4 Summary part II

This second part of the thesis indicates that in response to the second research question (see section 1.2 Aim):

- An inner electrode with sufficient conductivity can be introduced during melt spinning, by using a CB/polymer compound as core
- Poling can be carried out in a contact mode, with a CB/polymer compound or silver paint as outer electrode, or by corona discharge, with no outer electrode
- The most important parameter for a high polarisation is a high applied voltage
- Poling is most efficiently carried out at a temperature around 60°C, but polarisation is achieved also after poling at room temperature
- Corona poling can be carried out continuously, in-line with the spinning process, by adding a long poling channel and connecting the core compound melt to (electrical) ground

5. Putting the piezoelectric fibres to work

An application for the piezoelectric fibres was suggested in Paper V; by strapping a woven sensor around the chest it was possible to register heartbeat and breathing (Fig. 30). This could be a comfortable option for long-time monitoring. Energy harvesting, i.e. using the fibres as very small power supplies, was also considered. The maximum power output was estimated to be 15 nW from a yarn of 25 mm length.

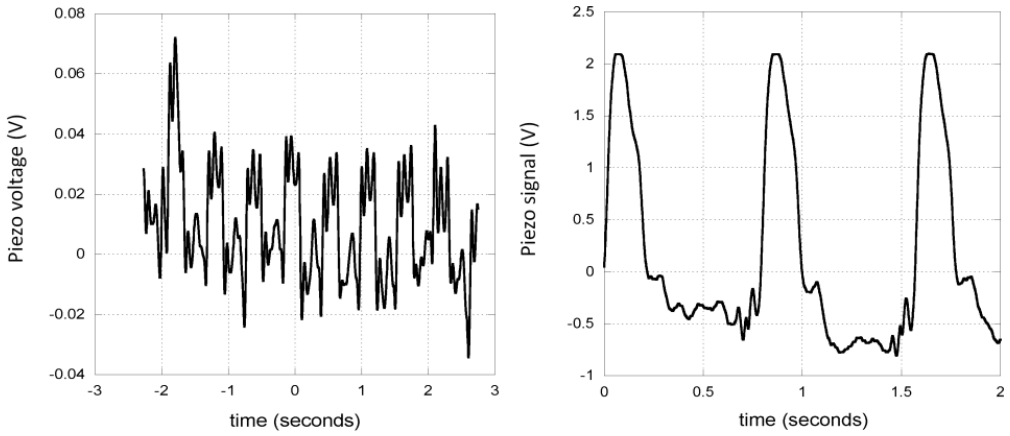

Figure 30 *Heartbeat signals generated from the piezoelectric fibres in a woven fabric strapped around the chest of a person holding his breath: raw signal (left) and filtered and amplified signal (right) [Paper V]*

Further, a demonstrator has been manufactured by embroidering a number of piezoelectric fibres on to a knitted glove, using couch stitch. The fibres thus constitute motion and temperature sensors in three positions (Fig. 31); the index finger joint, the back of the hand and on the tip of the thumb. Preliminary experiments[3] confirm that the sensors clearly register motion such as bending of the index finger and clenching of the fist, as well as the impact from tapping the thumb on a table surface (Fig. 32). The pyroelectric effect in the fibres was also confirmed by using the thumb sensor to register temperature variation; pressing the thumb to a bag of ice or to a cup of nearly boiling water produced the signals shown in Figure 33.

[3] The output signals from each fibre were measured with a USB oscilloscope PicoScope 2204, from Pico Technology (UK), and registered using the PicoScope software.

Figure *31 Demonstrator glove with 2 piezoelectric threads sewn onto the back of the hand (left image) and 1 piezoelectric thread sewn on to the palm of the hand (right image). There are also 8 light emitting diodes (LEDs) attached to the glove, which were not electrically connected at this stage.*

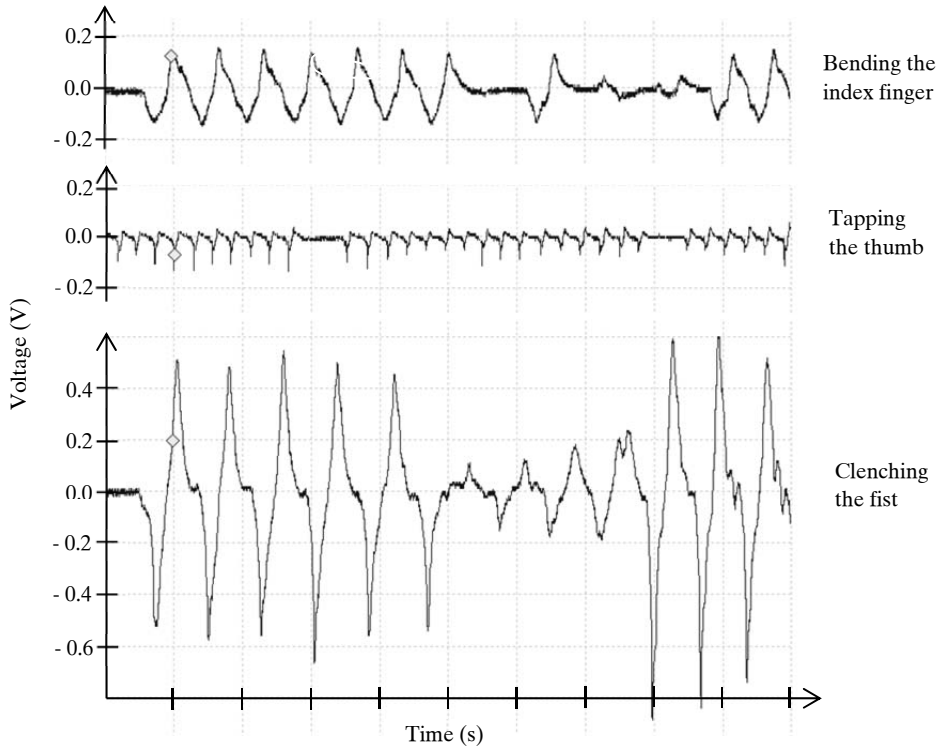

Figure 32 *Piezoelectric output voltage from the glove sensors as a function of time. The x-axis is common for all signals, its scale is 1 s/div. The sensors were activated by repetetive motions with varying amplitudes.*

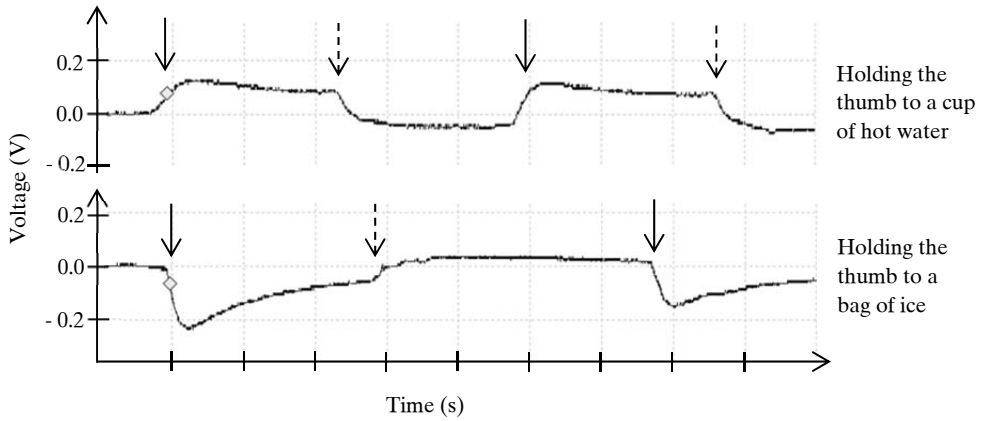

Figure 33 *Pyroelectric output from the glove sensors as a function of time. The x-axis is common and its scale is 1 s/div. The thumb was lightly pressed (indicated by the full arrows) to the hot/cold objects, held there for a few seconds and then removed (indicated by the dashed arrows).*

Piezoelectric fibres should be highly interesting for use in smart textiles; structures that can interact with their environment and/or their wearer. Recent publications demonstrate a diversity of applications for smart textiles ranging from textile electrodes for monitoring heart activity [105], brain activity [106] and bio impedance (for assessing body composition) [107] to interactive textile structures that change their pattern or shape [108-110] after user input. In these examples, textile structures were developed using commercially available fibres, yarns, colours and coatings.

With our piezoelectric fibres, "smartness" is introduced in the smallest component of a textile. Being able to sense temperature and pressure as well as motion, they bring us a step closer to actually having textiles that resemble our skin as once suggested by Tao [111]:

"*It would be wonderful to have clothing like our skin, which is a layer of smart material. The skin has sensors which can detect pressure, pain, temperature, etc. Together with our brain, it can function intelligently with environmental stimuli.* "

6. Conclusions

This work presented successful melt spinning and characterisation of piezoelectric fibres, using the piezoelectric polymer PVDF. The experimental studies showed that the melt spinning parameters greatly influence the formation of β phase crystallinity, which is necessary for the piezoelectric activity. In summary, the spinning process must include cold drawing, and the draw ratio should be as high as possible. Cold drawing is preferably carried out at a temperature between 70°C and 90°C. It was also shown that the addition of carbon nanotubes can increase the β phase content, but only under certain processing conditions which include ultrasonication in a solvent.

Once the β phase is introduced, the fibres must be equipped with electrodes and polarised. This work showed that an inner electrode with a sufficient degree of electrical conductivity can be introduced during melt spinning, by spinning bicomponent fibres with a CB/polymer compound as core and PVDF as sheath. Poling was carried out both in contact mode and using corona discharge. In both methods, the most important parameter for efficient polarisation was a high applied voltage. The optimal temperature for contact poling was found to be around 60°C. A method was developed for continuous poling, where corona discharge is applied to the fibres in-line with the spinning process.

The final fibres were shown to be highly sensitive to motion, impact and temperature. They should be interesting for use as miniature sensors or to produce smart textiles, where they can for example be integrated into clothing for comfortable monitoring of heartbeat or movement.

7. Suggestions for future work

This work can be continued in several directions, a few suggestions are given here.

- The addition of small amounts (below the percolation threshold) of carbon nanotubes could be evaluated as means to enhance the polarisability and final piezoelectric properties of PVDF.
- An increase in core conductivity should have a positive effect on the polarisability and increase the potential power output from the fibres. A simple first step towards increasing the core conductance could be to increase the core volume in the fibres.
- Producing monofilament bicomponent fibres instead of multifilament should result in fibres with more uniform geometries, which should in turn facilitate poling and give more reproducible piezoelectric properties.
- The application of the outer electrode remains to be explored; its formation will affect a sensor's mechanical properties as well as its response time. There exist a number of traditional textile production methods that could be useful such as coating with a conductive polymer compound, and twisting or weaving with conductive yarns.
- The practical applications for the piezoelectric fibres may be found in diverse areas such as medicine, acoustics, construction, sports *etc.*, and need to be discussed with expertise from these areas.

Acknowledgements

First of all, I would like to thank all my **colleagues** at the School of Textiles at the University of Borås (HB), at the Department for Materials and Manufacturing Technology at Chalmers University of Technology (CTH) and in the polymer group at the School of Engineering, HB, for providing a great working atmosphere, and for moral as well as practical support during my many times of absence due to maternity leave.

I especially want to express my gratitude to my supervisor **Bengt Hagström** at Swerea IVF/CTH for providing a fruitful combination of trust, critique and expertise; my co-supervisor **Pernilla Walkenström** at Swerea IVF for being there in times of need and my examiner **Mikael Rigdahl** at CTH for careful guidance through the final stages of my studies, and for providing such a good doctoral education through the Materials Science graduate school. Many thanks also to my former supervisors: **Rodney Rychwalski** at CTH for his patient support and **Hans Bertilsson** at HB for convincing encouragement.

Further, I am most grateful to all my co-authors and especially **Erik Nilsson** at Swerea IVF, **Christer Johansson** and **Christian Jonasson** at Acreo Swedish ICT for a fruitful and always pleasant collaboration; **Martin Stråål** and **Zengwei Guo** at Swerea IVF for their contributions to this research project; **Urban Jelvestam** at CTH for support and education on X-ray diffraction; and **Benjamin Glauß** at the RWTH Aachen University for providing the supplementary X-ray analysis. I also wish to thank **Mikael Skrifvars** at the School of Engineering at HB for providing such a well-equipped polymer lab, and **Haike Hilke** for supporting this lab in the best way.

The financial support for this research from the **University of Borås**, **Vinnova** via **Smart Textiles** and **the Swedish Foundation for Strategic Research (SSF)** via **LEF-TEX** is gratefully acknowledged. Also, thanks to **Solvay Solexis** for supplying polymer for the first trials free of charge.

Finally, I am as ever grateful to my loved ones, **Stefan, Alvar, August and Olle**, for being the best family I could possibly have wished for.

REFERENCES

1. Fukada, E., *History and Recent Progress in Piezoelectric Polymers*. IEEE Transactions on Ultrasonics, Ferroelectrics, and Frequency Control, 2000. **47**(6): p. 1277-1290.
2. Callister, J., William D., *Materials science and engineering an introduction*. 6th ed2003, New York, NY: John Wiley & Sons, Inc.
3. Kawai, H., *The piezoelectricity of poly(vinylidene fluoride)*. Japanese Journal of Applied Physics, 1969. **8**: p. 975-976.
4. Scheinbeim, J.I., J.W. Lee, and B.A. Newman, *Ferroelectric Polarization Mechanisms in Nylon 11*. Macromolecules, 1992. **25**: p. 3729-3732.
5. Tajitsu, Y., *Basic study on controlling piezoelectric motion of chiral polymeric fiber*. IEEE Transactions on Dielectrics and Electrical Insulation, 2010. **17**(4): p. 1050-1055.
6. Sensor Products Division, M.S., USA, *Piezo Film Sensors Technical Manual*, 1999.
7. Wang, F., et al., *Unconstrained cardiorespiratory monitor for premature infants*. International Journal of Applied Electromagnetics & Mechanics, 2007. **25**: p. 469-475.
8. Wang, F., M. Tanaka, and S. Chonan, *A PVDF piezopolymer sensor for unconstrained cardiorespiratory monitoring during sleep*. International Journal of Applied Electromagnetics & Mechanics, 2002. **16**: p. 181-188.
9. Choi, S. and Z. Jiang, *A novel wearable sensor device with conductive fabric and PVDF film for monitoring cardiorespiratory signals*. Sensors and Actuators A: Physical, 2006. **128**(2): p. 317-326.
10. Mateu, L. and F. Moll, *Appropriate charge control of the storage capacitor in a piezoelectric energy harvesting device for discontinuous load operation*. Sensors and Actuators A: Physical, 2006. **132**: p. 302-310.
11. *Solef & Hylar PVDF Design and Processing Guide*2006: Solvay Solexis.
12. Quig, J.B., *Technical Developments Leading to Present Man-Made Fibers*. Textile Research Journal, 1953. **23**: p. 280-288.
13. Hill, R., *Synthetic fibres in prospect and retrospect*. Journal of the Society of Dyers and Colourists, 1952. **68**: p. 158-168.
14. Whinfield, J.R., *The development of Terylene*. Textile Research Journal, 1953. **23**: p. 289-293.
15. Quig, J.B. and R.W. Dennison, *Functional Properties of Synthetics*. Industrial and engineering chemistry, 1952. **44**(9): p. 2176-2183.
16. Erlich, V.L., *Polyolefin Fibers and Polymer Structure*. Textile Research Journal, 1959. **29**: p. 679-686.
17. Ziabicki, A., *Fundamentals of fibre formation*. First ed1976, Bath: John Wiley & Sons.
18. Sisson, W.A. and F.F. Morehead, *The Skin Effect in Crimped Rayon*. Textile Research Journal, 1953. **23**: p. 152-157.
19. Fitzgerald, W.E. and J.P. Knudsen, *Mixed-stream Spinning of Bicomponent Fibers*. Textile Research Journal, 1967. **37**: p. 447-453.
20. Rabe, R.L., B.J. Collier, and J.R. Collier, *Processability and Properties of a Rayon/Nylon Composite Fiber*. Textile Research Journal, 1988. **58**: p. 735-742.
21. Walczak, Z.K., *Processess of fiber formation*2002, Amsterdam, NY: Elsevier.
22. Ide, Y. and J.L. White, *The spinnability of polymer fluid filaments*. Journal of Applied Polymer Science, 1976. **20**(9): p. 2511-2531.
23. White, J.L. and Y. Ide, *Instabilities and failure in elongational flow and melt spinning of fibers*. Journal of Applied Polymer Science, 1978. **22**(11): p. 3057-3074.
24. Laun, H.M. and H. Schuch, *Transient elongational viscosities and drawability of polymer melts*. Journal of Rheology, 1989. **33**(1): p. 119-175.

25. Tadmor, Z. and C.G. Gogos, *Principles of polymer processing*. 2nd ed2006, New York: John Wiley & Sons.
26. Ziabicki, A. and K. Kedzierska, *Studies on the Orientation Phenomena by Fiber Formation from Polymer Melts. Part I. Preliminary Investigations on Polycapronamide.* Journal of Applied Polymer Science, 1959. **II**(4): p. 14-23.
27. Ziabicki, A. and K. Kedzierska, *Studies on the Orientation Phenomena by Fiber Formation from Polymer Melts. IV. Effect of Molecular Structure on Orientation. Polyethylene and Polystyrene.* Journal of Applied Polymer Science, 1962. **VI**(21): p. 361-367.
28. Katayama, K., T. Amano, and K. Nakamura, *Structural formation during melt spinning process.* Kolloid-Zeitschrift und Zeitschrift für Polymere, 1967. **226**(2): p. 125-134.
29. Dees, J.R. and J.E. Spruiell, *Structure Development During Melt Spinning of Linear Polyethylene Fibers.* Journal of Applied Polymer Science, 1974. **18**: p. 1053-1078.
30. Hirahata, H., et al., *On-line measurements of orientation induced crystallization of PET during high speed spinning.* Polymer, 1996. **37**(23): p. 5131-5137.
31. Samon, J.M., et al., *Structure Development during the Melt Spinning of Polyethylene and Poly(vinylidene fluoride) Fibers by in Situ Synchrotron Small- and Wide-Angle X-ray Scattering Techniques.* Macromolecules, 1999. **32**(24): p. 8121-8132.
32. Schultz, J., *Polymer materials science*1974, New Jersey: Prentice-Hall, Inc.
33. Séguéla, R., *On the natural draw ratio of semi-crystalline polymers: Review of the mechanical, physical and molecular aspects.* Macromolecular Materials and Engineering, 2007. **292**: p. 235-244.
34. Gregorio, R.J., *Determination of the Crystalline Phases of Poly(vinylidene fluoride) Films Prepared at Different Conditions.* Journal of Applied Polymer Science, 2006. **100**: p. 3272-3279.
35. Wang, Y., M. Cakmak, and J.L. White, *Structure development in melt spinning poly(vinylidene fluoride) fibers and tapes.* Journal of Applied Polymer Science, 1985. **30**: p. 2615-2632.
36. Wang, Y.D. and M. Cakmak, *Hierarchical structure gradients developed in injection-molded PVDF and PVDF-PMMA blends. I. Optical and thermal analysis.* Journal of Applied Polymer Science, 1998. **68**: p. 909-926.
37. Hattori, T., M. Hikosaka, and H. Ohigashi, *The crystallization behaviour and phase diagram of extended-chain crystals of poly(vinylidene fluoride) under high pressure.* Polymer, 1996. **37**(1): p. 85-91.
38. Bershtein, V.A. and V.M. Egorov, *Differential Scanning Calorimetry of Polymers*. First English edition ed1994, Midsomer Norton: Ellis Horwood Limited.
39. Du, C.-H., B.-K. Zhu, and Y.-Y. Xu, *Effects of stretching on crystalline phase structure and morphology of hard elastic PVDF fibers.* Journal of Applied Polymer Science, 2007. **104**(4): p. 2254-2259.
40. Mohammadi, B., A.A. Yousefi, and S.M. Bellah, *Effect of tensile strain rate and elongation on crystalline structure and piezoelectric properties of PVDF thin films.* Polymer Testing, 2007. **26**: p. 42-50.
41. Sobhani, H., M. Razavi-Nouri, and A.A. Yousefi, *Effect of flow history on Poly(vinylidine fluoride) crystalline phase transformation.* Journal of Applied Polymer Science, 2007. **104**: p. 89-94.
42. Wu, J., et al., *In-Situ Simultaneous Synchrotron Small- and Wide-Angle X-ray Scattering Measurement of Poly(vinylidene fluoride) Fibers under Deformation.* Macromolecules, 2000. **33**(5): p. 1765-1777.
43. Kang, Y.A., et al., *Development of a fiber structure in poly(vinylidene fluoride) by a CO_2 laser-heated drawing process.* Polymer Journal, 2010. **42**: p. 657-662.

44. Steinmann, W., et al., *Structure, Properties, and Phase Transitions of Melt-Spun Poly(vinylidene fluoride) Fibers.* Journal of Applied Polymer Science, 2011. **120**: p. 21-35.
45. Sajkiewicz, P., A. Wasiak, and Z. Goclowski, *Phase transitions during stretching of poly(vinylidene fluoride).* European Polymer Journal, 1999. **35**: p. 423-429.
46. Guo, H., et al., *In-situ synchrotron SAXS and WAXS investigations on deformation and α - β transformation of uniaxial stretched poly(vinylidene fluoride).* CrystEngComm, 2013. **15**: p. 1597-1606.
47. Matsuda, Y., Y. Ota, and S. Tasaka, *Changes in the Melting Temperature and Crystal Structure of Poly(Vinylidene Fluoride) by Knotting.* Journal of Applied Polymer Science, 2013. **128**(5): p. 3107-3112.
48. Van Mele, B. and E. Verdonck, *Physio-chemical characterization of the fibre/matrix interaction in polyethylene fibre/epoxy matrix composites. Part 1. Characterization with DSC.* Composite Interfaces, 1995. **3**(2): p. 83-100.
49. Min, B.G., et al., *Polymer/carbon nanotube composite fibers - An overview*, in *Functional Composites of Carbon Nanotubes and Applications*, K.-P. Lee, A.I. Gopalan, and F.D.S. Marquis, Editors. 2009, Transworld Research Network: Kerala, India. p. 43-73.
50. Zhao, Z., et al., *Electrical conductivity of poly(vinylidene fluoride)/carbon nanotube composites with a spherical substructure.* Carbon, 2009. **47**: p. 2118-2120.
51. Almasri, A., et al., *Characterization of Solution-Processed Double-Walled Carbon Nanotube/Poly(vinylidene fluoride) Nanocomposites.* Macromolecular Materials and Engineering, 2008. **293**: p. 123-131.
52. Carabineiro, S.A., et al., *Effect of the carbon nanotube surface characteristics on the conductivity and dielectric constant of carbon nanotube/poly(vinylidene fluoride) composites.* Nanoscale Research Letters, 2011. **6**(302): p. 1-5.
53. Levi, N., et al., *Properties of Polyvinylidene Difluoride-Carbon nanotube blends.* Nano letters, 2004. **4**(7): p. 1267-1271.
54. Yu, S., et al., *Formation Mechanism of β-phase in PVDF/CNT Composite Prepared by the Sonication Method.* Macromolecules, 2009. **42**: p. 8870-8874.
55. Guo, Z., et al., *Melt spinning of PVDF fibers with enhanced beta phase structure.* Journal of Applied Polymer Science, 2013.
56. Bohlén, M., *Computational studies of poly(vinylidene fluoride) and poly(vinylidene fluoride) - single wall carbon nanotube composites*, in *School of Engineering, University of Borås*2012, Chalmers University of Technology: Gothenburg, Sweden.
57. Laxminarayana, K. and N. Jalili, *Functional nanotube-based textiles: pathway to next generation fabrics with enhanced sensing capabilities.* Textile Research Journal, 2005. **75**(9): p. 670-680.
58. Yuan, J.-K., et al., *Giant dielectric permittivity nanocomposites: Realizing true potential of pristine carbon nanotubes in polyvinylidene fluoride matrix through an enhanced interfacial interaction.* The Journal of Physical Chemistry C, 2011. **115**: p. 5515-5521.
59. Jadidian, B., et al., *Processing of Piezoelectric Fiber/Polymer Composites with 3-3 Connectivity.* Journal of Electroceramics, 2002. **8**: p. 209-214.
60. Mohammadi, F., A. Khan, and R.B. Cass. *Power generation from piezoelectric lead zirconate titanate fiber composites.* in *Mat. Res. Soc. Symp. Proc.* 2003. Materials Research Society.
61. Sato, H., et al. *Metal Core Piezoelectric Complex Fiber and Application for Smart System.* in *Mater. Res. Soc. Symp.* 2006. Materials Research Society.
62. Pini, N., et al., *In situ growth of interdigitated electrodes made of polypyrrole for active fiber composites.* Polymers for Advanced Technologies, 2007. **18**(3): p. 249-253.

63. Wu, A.Y., et al., *Morphology, polymorphism behavior and molecular orientation of electrospun poly(vinylidene fluoride) fibers.* Polymer, 2007. **48**: p. 512-521.
64. Huang, S., et al., *Electrospinning of Polyvinylidene Difluoride with Carbon Nanotubes: Synergistic Effects of Extensional Force and Interfacial Interaction on Crystalline Structures.* Langmuir, 2008. **24**: p. 13621-13626.
65. Chang, C., et al., *Direct-write piezoelectric polymeric nanogenerator with high energy conversion efficiency.* Nano letters, 2010. **10**: p. 726-731.
66. Andrew, J.S. and D.R. Clarke, *Effect of electrospinning on the ferroelectric phase content of polyvinylidene difluoride fibers.* Langmuir, 2008. **24**: p. 670-672.
67. Wang, Y.R., et al., *A flexible piezoelectric force sensor based on PVDF fabrics.* Smart Mater. Struct., 2011. **20**: p. 1-7.
68. Egusa, S., et al., *Multimaterial piezoelectric fibres.* Nature materials, 2010. **9**: p. 643-648.
69. Walter, S., et al., *Characterisation of piezoelectric PVDF monofilaments.* Materials Technology, 2011. **26**(3): p. 140-145.
70. Ito, S., et al., *Sensing Using Piezoelectric Chiral Polymer Fiber.* Japanese Journal of Applied Physics, 2012. **51**: p. 09LD16-1--5.
71. Balberg, I., *A comprehensive picture of the electrical phenomena in carbon black - polymer composites.* Carbon, 2002. **40**: p. 139-143.
72. Foulger, S.H., *Electrical properties of composites in the vicinity of the percolation threshold.* Journal of Applied Polymer Science, 1999. **72**: p. 1573-1582.
73. Hagström, B. *Electrical Conductivity and Processability of Mono-component and Bi-component Melt Spun Polypropylene Fibres Containing a Highly Conductive Carbon Black.* in *Ambience08*. 2008. Borås, Sweden: Högskolan i Borås, CTF.
74. Stråat, M., et al., *Melt spinning of conducting polymeric composites containing carbonaceous fillers.* Journal of Applied Polymer Science, 2011. **119**: p. 3264-3272.
75. Stråat, M., M. Rigdahl, and B. Hagström, *Conducting Bicomponent Fibers Obtained by Melt Spinning of PA6 and Polyolefins Containing High Amounts of Carbonaceous Fillers.* Journal of Applied Polymer Science, 2012. **123**: p. 936-943.
76. Alig, I., et al., *Destruction and formation of a carbon nanotube network in polymer melts: Rheology and conductivity spectroscopy.* Polymer, 2008. **49**: p. 3524-3532.
77. Ferreira, A., et al., *Extrusion of poly(vinylidene fluoride) filaments: effect of the processing conditions and conductive inner core on the electroactive phase content and mechanical properties.* Journal of Polymer Research, 2011. **18**(6): p. 1653-1658.
78. Glauss, B., et al., *Spinnability and Characteristics of Polyvinylidene Fluoride (PVDF)-based Bicomponent Fibes with a Carbon Nanotube (CNT) Modified Polypropylene Core for Piezoelectric Applications.* Materials, 2013. **6**: p. 2642-2661.
79. Day, G.W., et al., *Effects of poling conditions on responsivity and uniformity of polarization of PVF_2 pyroelectric detectors.* Applied Physics Letters, 1974. **24**(10): p. 456-458.
80. Blevin, W.R., *Poling rates for films of polyvinylidene fluoride.* Applied Physics Letters, 1977. **31**(1): p. 6-8.
81. DeRossi, D., et al., *Method of evaluating the thermal stability of the pyroelectric properties of polyvinylidene fluoride: Effects of poling temperature and field.* J. Appl. Phys., 1982. **53**: p. 6520-6525.
82. Wang, T.T., J.M. Herbert, and A.M. Glass, eds. *The applications of ferroelectric polymers.* 1988, Kluwer Academic Publishers.
83. Wang, T.T. and H. von Seggern, *High electric field poling of electroded poly(vinylidene fluoride) at room temperature.* J. Appl. Phys., 1983. **54**(8): p. 4602-4604.

84. Giacometti, J.A., S. Fedosov, and M.M. Costa, *Corona Charging of Polymers: Recent Advances on Constant Current Charging.* Brazilian Journal of Physics, 1999. **29**(2): p. 269-279.
85. Southgate, P.D., *Roomtemperature poling and morphology changes in pyroelectric polyvinylidene fluoride.* Applied Physics Letters, 1976. **28**: p. 250-252.
86. Das Gupta, D.K. and K. Doughty, *Corona charging and the piezoelectric effect in polyvinylidene fluoride.* J. Appl. Phys., 1978. **49**: p. 4601-4603.
87. Giacometti, J.A., et al., *Study of poling behavior of biaxially stretched poly(vinylidene fluoride) films using the constant-current corona triode.* J. Appl. Phys., 1995. **78**(9): p. 5597-5603.
88. Fukada, E. and S. Takashita, *Piezoelectric effect in polarized poly(vinylidene fluoride).* Japanese Journal of Applied Physics, 1969. **8**: p. 960.
89. Naegele, D. and D.Y. Yoon, *Orientation of crystalline dipoles in poly(vinylidene fluoride) films under electric field.* Applied Physics Letters, 1978. **33**(2): p. 132-134.
90. Rollik, D., S. Bauer, and R. Gerhard-Multhaupt, *Separate contributions to the pyroelectricity in poly(vinylidene fluoride) from the amorphous and crystalline phases, as well as from their interface.* Journal of Applied Physics, 1999. **85**(6): p. 3282-3288.
91. Murayama, N., et al., *Persistent Polarization in Poly(vinylidene Fluoride). II. Piezoelectricity of Poly(vinylidene Fluoride) Thermoelectrets.* Journal of Polymer Science: Polymer Physics Edition, 1975. **13**: p. 1033-1047.
92. Wang, T.T., et al., *Dielectric hysteresis behavior in form I poly(vinylidene fluoride).* J. Appl. Phys., 1987. **62**(11): p. 4514-4517.
93. Gomes, J., et al., *Influence of the beta-phase content and degree of crystallinity on the piezo- and ferroelectric properties of poly(vinylidene fluoride).* Smart Mater. Struct., 2010. **19**: p. 1-7.
94. Kepler, R.G. and R.A. Anderson, *Ferroelectricity in polyvinylidene fluoride.* J. Appl. Phys., 1978. **49**(3): p. 1232-1235.
95. Büchtemann, A. and R. Schmolke, *Infrared spectroscopic investigation of poly(vinylidene fluoride) in an electric field.* Journal of Polymer Science Part B: Polymer Physics, 1991. **29**(10): p. 1299-1302.
96. Dvey-Aharon, H., T.J. Sluckin, and P.L. Taylor, *Kink propagation as a model for poling in poly(vinylidene fluoride).* Physical Review B, 1980. **21**(8): p. 2700-3707.
97. Tamura, M., et al., *Some aspects of piezoelectricity and pyroelectricity in uniaxially stretched poly(vinylidene fluoride).* Journal of Applied Physics, 1977. **48**(2): p. 513-521.
98. Guan, F., et al., *Effects of Polymorphism and Crystallite Size on Dipole Reorientation in Poly(vinylidene fluoride) and Its Random Copolymers.* Macromolecules, 2010. **43**: p. 6739-6748.
99. McKinney, J.E., G.T. Davis, and M.G. Broadhurst, *Plasma poling of poly(vinylidene fluoride): Piezo- and pyroelectric response.* J. Appl. Phys., 1980. **51**(3): p. 1676-1681.
100. Scheinbeim, J.I., et al., *Poling-Time Dependence of the Field-Induced Phase Transition and Piezoelectric Response of Poly(vinylidene Fluoride) Films.* Journal of Polymer Science: Polymer Physics Edition, 1980. **18**: p. 2271-2276.
101. Womes, M., E. Bihler, and W. Eisenmenger, *Dynamics of Polarization Growth and Reversal in PVDF Films.* IEEE Transactions on Electrical Insulation, 1989. **24**(3): p. 461-468.
102. Eisenmenger, W., H. Schmidt, and B. Dehlen, *Space Charge and Dipoles in Polyvinylidenefluoride.* Brazilian Journal of Physics, 1999. **29**(2): p. 295-305.
103. Bihler, E., et al. *Influence of charge injection on the formation of remanent polarization in P(VDF-TrFE) copolymers.* in *IEEE Annual Report Conf. Electr. Insul. Diel. Phenom.* 1990. Piscataway.

104. Eliasson, S., *On TSD in PVDF in the temperature range -60°C to 165°C. I.* J. Phys. D: Appl. Phys., 1985. **18**: p. 275-282.
105. Berglin, L., *Interactive Textile Structures Creating Multifunctional Textiles based on Smart Materials*, in *The Swedish School of Textiles*2008, University of Borås: Chalmers University of Technology, Göteborg.
106. Eriksson, S., et al. *3D Weaving Technique Applied in Long Term Monitoring of Brain Activity*. in *4th World Conference on 3D Fabrics and Their Applications*. 2012. Aachen: RWTH Aachen University, Aachen, Germany.
107. Márquez Ruiz, J.C., *Sensor-Based Garments that Enable the Use of Bioimpedance Technology: Towards Personalized Healthcare Monitoring*, in *School of Enginering*2013, University of Borås: KTH Royal Institute of Technology.
108. Worbin, L., *Designing dynamic textile patterns*, in *Swedish School of Textiles*2010, Högskolan i Borås: Chalmers University of Technology.
109. Persson, A., *Exploring Textiles as Materials for Interaction Design*, in *The Swedish School of Textiles*2013, University of Borås: Borås.
110. Zetterblom, M., *Textile Sound Design*, in *The Swedish School of Textiles*2011, The University of Borås: Chalmers University of Technology, Gothenburg, Sweden.
111. Tao, X., *Smart fibres, fabrics and clothing*2001: Woodhead Publishing.